# An ensemble of specifically targeted proteins stabilizes cortical microtubules in the human parasite *Toxoplasma gondii*

Jun Liu[a,*], Yudou He[a,*], Imaan Benmerzouga[b], William J. Sullivan, Jr.[b], Naomi S. Morrissette[c], John M. Murray[a], and Ke Hu[a]

[a]Department of Biology, Indiana University, Bloomington, IN 47405; [b]Department of Pharmacology and Toxicology and Department of Microbiology and Immunology, Indiana University School of Medicine, Indianapolis, IN 46202; [c]Department of Molecular Biology and Biochemistry, University of California, Irvine, Irvine, CA 92697

**ABSTRACT** **Although all microtubules within a single cell are polymerized from virtually identical subunits, different microtubule populations carry out specialized and diverse functions, including directional transport, force generation, and cellular morphogenesis. Functional differentiation requires specific targeting of associated proteins to subsets or even subregions of these polymers. The cytoskeleton of *Toxoplasma gondii*, an important human parasite, contains at least five distinct tubulin-based structures. In this work, we define the differential localization of proteins along the cortical microtubules of *T. gondii*, established during daughter biogenesis and regulated by protein expression and exchange. These proteins distinguish cortical from mitotic spindle microtubules, even though the assembly of these subsets is contemporaneous during cell division. Finally, proteins associated with cortical microtubules collectively protect the stability of the polymers with a remarkable degree of functional redundancy.**

**Monitoring Editor**
Kerry S. Bloom
University of North Carolina

Received: Nov 3, 2015
Revised: Dec 7, 2015
Accepted: Dec 8, 2015

## INTRODUCTION

Microtubules are universally found in eukaryotic cells, where they are organized into functionally distinct structures such as the mitotic spindle, tracks for vesicular transport, and the basal body and associated flagellar axoneme (Pollister, 1939; Bernhard and De Harven, 1956; Szollosi, 1964; Inoué and Sato, 1967; Inoué *et al.*, 1975; Salmon, 1975; Gibbons, 1981; Gilbert *et al.*, 1985; Sheetz *et al.*, 1986; Stebbings and Hunt, 1987; Huitorel, 1988; Sawin and Mitchison, 1991; Johnson and Rosenbaum, 1992; Salisbury, 1995; Preble *et al.*, 2000; Dutcher, 2003; Walczak and Heald, 2008; Carvalho-Santos *et al.*, 2011). Because all microtubules are built with essentially the same core α-β tubulin heterodimers, how these distinct structures are established and maintained is an important question in biology. This problem is particularly intriguing considering that many proteins have to be specifically targeted to subsets or subregions of microtubules to generate different types of structures that coexist in the same cell. In the protozoan parasite *Toxoplasma gondii*, there are at least five discrete tubulin-based structures, including the conoid, cortical microtubules, intraconoid microtubules, and centrioles, as well as a spindle in replicating parasites (Figure 1; Chobotar and Scholtyseck, 1982; Nichols and Chiappino, 1987; Morrissette, 1995; Morrissette and Sibley, 2002a; Hu *et al.*, 2002b; Swedlow *et al.*, 2002). It is therefore an excellent model system for understanding the differential targeting of microtubule-associated proteins.

*T. gondii* belongs to the phylum Apicomplexa, a group of ~6000 parasites that includes a number of important human pathogens (Levine, 1988). The most notorious members of this phylum are *Plasmodium* spp., the malarial parasites. More than half a million people, mostly children younger than the age of 5 yr, die from malaria each year (World Health Organization, 2014). In contrast to the malarial parasites, which are restricted by the geographic distribution of competent mosquito vectors, *T. gondii* is found worldwide.

This article was published online ahead of print in MBoC in Press (http://www.molbiolcell.org/cgi/doi/10.1091/mbc.E15-11-0754) December 17, 2015.

*These authors contributed equally.

Address correspondence to: Ke Hu (kehu@indiana.edu).

Abbreviations used: eGFP, enhanced green fluorescent protein; FACS, fluorescence-activated cell sorting; FRAP, fluorescence recovery after photobleaching; HFF, human foreskin fibroblast; IMC, inner membrane complex; SPM1, subpellicular microtubule protein 1; TLAP, TrxL1-associated protein; TrxL1, thioredoxin-like protein 1.

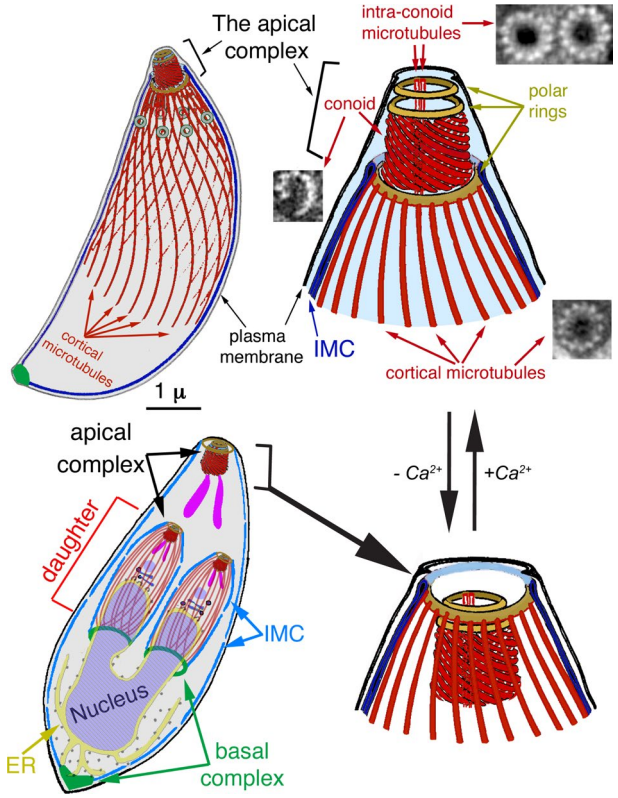


FIGURE 1: Diagrams of the *T. gondii* cytoskeleton. Highlighted in red are several tubulin-containing structures in *T. gondii*, including 22 cortical microtubules, two intraconoid microtubules, and 14 conoid fibers, which are novel tubulin polymers. Also shown are electron microscopic cross-sections of the cortical and intraconoid microtubules and a conoid fiber (Hu *et al.*, 2002b). IMC, inner membrane complex. Bottom left, diagram of a replicating parasite, with daughter parasites being built inside the mother. Note that the cortical microtubules are present in the mother but not shown to avoid clutter. At this stage, most membrane-bound organelles have been produced or duplicated and partitioned into daughters. For simplicity, only the Golgi stack (dark blue) and apicoplast (a plastid-like organelle, light purple) and rhoptries (one of the specialized organelles for invasion; purple) are shown for daughters. The apical complex is typically retracted in intracellular parasites (bottom). An increase in concentration of cytoplasmic calcium triggers the switch from the retracted to the extended state (top).

Approximately one-third of the global population are carriers of this parasite (Luder *et al.*, 2001; Dubey, 2008; Torgerson and Mastroiacovo, 2013). The widespread prevalence of *T. gondii* is largely due to its ability to invade and proliferate in any warm-blooded animal. Humans can acquire *T. gondii* infection through contaminated food (mainly undercooked meat), water, and soil (Frenkel, 1973; Beazley and Egerman, 1998; Dubey, 1998, 2008) or through contact with highly infectious sporocysts from the feces of cats, the only definitive host of this parasite (Dubey *et al.*, 1970; Dubey, 1998, 2008). Infection of a pregnant female often leads to fetal infection via placental transfer, with consequent severe congenital neurological defects (Dunn *et al.*, 1999; Montoya and Liesenfeld, 2004). *T. gondii* infections are asymptomatic in healthy nonpregnant individuals because parasite proliferation is held in check by the immune system, although parasites persist for the life of the host as dormant cysts in the brain, skeletal muscle, and cardiac muscle (Dubey, 2008; Sullivan and Jeffers, 2012). However, infections in immunocompromised individuals have devastating consequences, including the development of life-threatening toxoplasmic encephalitis, because latent parasites can reactivate, escape from cysts, proliferate rapidly, and severely damage tissues (Luft and Remington, 1992; Luft *et al.*, 1993).

To successfully infect a host, both malarial parasites and *T. gondii* need to penetrate multiple layers of tissues, establish vacuoles in host cells, replicate, escape from the resource-depleted host cell, and then disseminate. Subsequently they invade new host cells to initiate additional rounds of invasion (Sibley *et al.*, 1994; Sibley, 2004; Pinder *et al.*, 2000; Hoff and Carruthers, 2002). The cytoskeleton of the parasite is essential to all of these steps. The motility of the parasite is powered by an actomyosin-based apparatus (Dobrowolski and Sibley, 1996; Dobrowolski *et al.*, 1997; Sibley *et al.*, 1998; Meissner *et al.*, 2002; Opitz and Soldati, 2002; Gaskins *et al.*, 2004; Egarter *et al.*, 2014), which is sandwiched between the plasma membrane and the inner membrane complex (IMC), a sheet of flattened vesicles joined by sutures that associates with the plasma membrane to form the parasite pellicle (Sheffield and Melton, 1968; Porchet and Torpier, 1977; Dubremetz and Torpier, 1978; Morrissette *et al.*, 1997). The IMC associates with a large number of cytoskeletal proteins that form the cortical cytoskeleton (Figure 1). These function to provide a rigid framework that the actomyosin machinery works against to power gliding motility and host cell invasion. The cytoskeleton is also essential for parasite replication. Apicomplexan parasites replicate by packaging nascent daughter buds within a mother. Nuclear division is coordinated with the formation of daughter buds, and the nuclear envelope remains intact during chromosome segregation. In *T. gondii*, the mitotic spindle is inserted into "spindle plaques" embedded in the nuclear envelope (Senaud, 1967; Chobotar and Scholtyseck, 1982) and is sensitive to inhibitors of tubulin polymerization. Little else is known about how the parasite mitotic spindle is assembled, due to the lack of appropriate markers. The emerging IMC and associated cortical cytoskeleton of daughter buds provide an essential framework for housing the de novo–synthesized secretory organelles used in host cell invasion, as well as for partitioning replicated organelles, including the Golgi apparatus, endoplasmic reticulum, apicoplast, mitochondrion, and nucleus (Figure 1; Sheffield and Melton, 1968; Hu *et al.*, 2002a; Morrissette and Sibley, 2002a; Nishi *et al.*, 2008). Assembly of the cortical cytoskeleton in daughter buds is tightly coupled to replication of centrioles: the polarized daughter cytoskeleton is initiated close to newly duplicated centrioles, suggesting a central role for the centrioles in templating the cortical cytoskeleton (Hu *et al.*, 2006; Hu, 2008). This hypothesis is strengthened by the discovery of a striated fiber assemblin (SFA) fiber that links the centrioles and emergent buds and is important for initiating assembly of the daughter cytoskeleton (Francia *et al.*, 2012).

One of the central components of the cortical cytoskeleton in apicomplexan parasites is a set of cortical (subpellicular) microtubules, which are built with great specificity. For instance, there are two or three cortical microtubules in erythrocytic-stage *Plasmodium falciparum* merozoites, 15 or 16 in *Plasmodium berghei* sporozoites, 22 in the asexual form of *T. gondii*, and 26 in *Eimeria*, a close relative of *Toxoplasma* in the subclass Coccidia (Vanderberg *et al.*, 1967; Dubremetz, 1973; D'Haese *et al.*, 1977; Nichols and Chiappino, 1987; Bannister and Mitchell, 1995; Fowler *et al.*, 1998). The organization of cortical microtubules in *T. gondii* has been well characterized by light and electron microscopy. They form a left-handed spiral extending from the apical end of the parasite to approximately two-thirds of the cell body length in mature parasites (Figure 1; Nichols and Chiappino, 1987; Morrissette *et al.*, 1997) and closely

associate with the IMC along their length throughout the cell cycle. Coordinated growth of cortical microtubules and the IMC during cell division is essential for packaging daughters inside the mother cell (Figure 1). Inhibition of microtubule growth by the depolymerizing drug oryzalin induces abnormal IMC assembly and aberrant morphology, and the resulting parasites are nonviable (Morejohn *et al.*, 1987; Stokkermans *et al.*, 1996; Shaw *et al.*, 2000; Morrissette and Sibley, 2002b; Morrissette *et al.*, 2004; Hu *et al.*, 2006; Hu, 2008). However, it is not known whether cortical microtubules are essential for maintaining the characteristic "banana" shape of adult parasites because mature cortical microtubules in living parasites are impervious to standard disassembly methods such as cold- or drug-induced depolymerization. For the same reason, the role of cortical microtubules in parasite motility has not been tested, although it was proposed that they might dictate the long-range directionality for the movement of apicomplexan parasites (Sinden, 1985), recently shown for *Toxoplasma* (Leung *et al.*, 2014) and *Plasmodium* (Kan *et al.*, 2014), to follow a left-handed helix in a matrix that permits three-dimensional movement.

Unlike the dynamic, labile, and idiosyncratically arranged microtubule cytoskeleton in mammalian cells, *T. gondii* cortical microtubules are exceptionally stable and have the same distribution in every cell. They do not display dynamic instability and are not depolymerized when the free tubulin concentration is drastically reduced by detergent extraction (Nichols and Chiappino, 1987; Morrissette *et al.*, 1997), which leads to rapid disassembly of vertebrate cell microtubule arrays. These polymers therefore not only are essential to the parasite but also distinguish the parasite from the host. By understanding the construction and function of these microtubules, we may potentially discover new parasite-specific drug targets for treating toxoplasmosis and other apicomplexan diseases. The unusual stability of cortical microtubules is likely due to parasite-specific microtubule-binding or -modifying proteins because the predominant α1- and β1-tubulin subunits that form these polymers are largely conserved relative to human tubulin homologues (>85% identity and 90% similarity). Indeed, earlier ultrastructural studies revealed that cortical microtubules are heavily decorated with associated proteins (Morrissette *et al.*, 1997; Hu *et al.*, 2002b), which we refer to as coating proteins. In parasites lacking SPM1, one of the first characterized microtubule-coating proteins in *T. gondii* (Tran *et al.*, 2012), cortical microtubules completely depolymerize upon cell lysis by detergent. More recently, we identified another novel protein, thioredoxin-like protein 1 (TrxL1), which is localized to both the cortical and intraconoid microtubule populations (Liu *et al.*, 2013; Supplemental Figure S1). The interaction between TrxL1 and cortical microtubules is dependent on SPM1. We used TrxL1 as the bait for immunoprecipitation and found several proteins in addition to SPM1. These include TrxL2, a homologue of TrxL1, as well as TrxL1-associated proteins 1–4 (TLAPs 1-4; Liu *et al.*, 2013), four proteins unrelated to each other in primary sequence. In our initial analysis, we ectopically expressed tagged TrxL2 and TLAP1 in *T. gondii* and demonstrated that both localize to the cortical microtubules (Liu *et al.*, 2013).

In this work, we report on several intriguing features of the microtubule cytoskeleton in the asexual form of *T. gondii*. First, cortical microtubules are differentially decorated with proteins along their length in a complex but defined pattern, which involves specific targeting of coating proteins to the forming cytoskeleton of the daughter. Second, the assembly of cortical microtubules is coordinated with that of the mitotic spindle both in space and time, revealing a cell cycle–dependent regulation of the communication between the nucleus and the cytosol. Finally, as an ensemble, the coating proteins protect the stability of cortical microtubules in a region-dependent manner and with a remarkable level of functional redundancy.

## RESULTS

### Differential assembly of coating proteins onto cortical microtubules

Two previously characterized proteins, TrxL1 (Supplemental Figure S1) and SPM1, both coat the entire length of cortical microtubules (Tran *et al.*, 2012; Liu *et al.*, 2013). In contrast, two proteins identified in our previous proteomic screen (Liu *et al.*, 2013), TLAP2 (TGGT1_232130; EuPathDB.org) and TLAP3 (TGGT1_235380), exhibit complex and distinct patterns along the polymers. Figure 2 shows the localization of fluorescently tagged TLAP2 and TLAP3 in knock-in lines created by double-crossover homologous recombination (Heaslip *et al.*, 2010, 2011; Liu *et al.*, 2013) in which the endogenous genes were replaced by the coding sequence for fluorescently tagged TLAP2 or TLAP3. Proceeding from the apical toward the basal end of the parasite, there are three identifiable regions with different TLAP2 occupancies: a ring-like structure marked by TLAP2, with an outer diameter of ~0.9 µm; a segment of TLAP2-free region (Figure 2, A and B, and Supplemental Video S1), which partially overlaps with an apical subdomain of the membrane cortex marked by ISP1 (Beck *et al.*, 2010); and the remaining expanse of cortical microtubules (~3–5 µm in length), which is coated with TLAP2. The distribution of TLAP3 is different and resembles an ~0.8 × 0.4–µm cone close to the apical end of the parasite (Figure 2C). In the intact parasite, it is difficult to resolve structural detail in this small region (Figure 2C), but in detergent-extracted extracellular parasites, in which the microtubules are splayed, TLAP3 is localized at the apical tips of the cortical microtubules (Figure 2D). In addition to the cortical microtubules, TLAP3 is also localized to the intraconoid microtubules (arrowheads, Figure 2D; also see Figure 1).

### Specific targeting to the apical section of cortical microtubules

Cortical microtubules are generated de novo when daughters form inside the mother during parasite replication (Figure 1). To determine whether subdomains of the protein coating we observed on cortical microtubules are established during or subsequent to daughter construction, we examined TLAP3 localization in parasites at different stages of replication in the *mNeonGreenFP-TLAP3* knock-in line (Figure 3). We found that TLAP3 labeling first appears in daughter buds as six or seven spots surrounding a central dot that is likely to be the intraconoid microtubules (Figure 3, insets). The recruitment of TLAP3 to the daughter cytoskeleton occurs early, before detection by immunofluorescence of IMC1 (Figure 3A), a component of the protein network underneath the IMC (Mann and Beckers, 2001; Mann *et al.*, 2002). Consistent with a previous observation (Chen *et al.*, 2015), TLAP3 is also detected in daughters before ISP1 (Figure 3A), a protein localized to the apical subdomain of the IMC (Beck *et al.*, 2010). As the daughters grow, the ISP1 labeling in the daughters lengthens from a narrow band close to the apex to a mantle extending well beyond the TLAP3 apical concentration (Figure 3, B–F). Thus structural differentiation of the coating on cortical microtubules is an integral part of the construction program and is established during the initial assembly of daughter cells.

When expressed from its endogenous promoter, TLAP3 is not detectable on the mitotic spindle, even though the assembly of the cortical microtubules and mitotic spindle occurs contemporaneously. Figure 4, Supplemental Video S2, and Supplemental Figure S1C show a series of images in which the cortical microtubules and

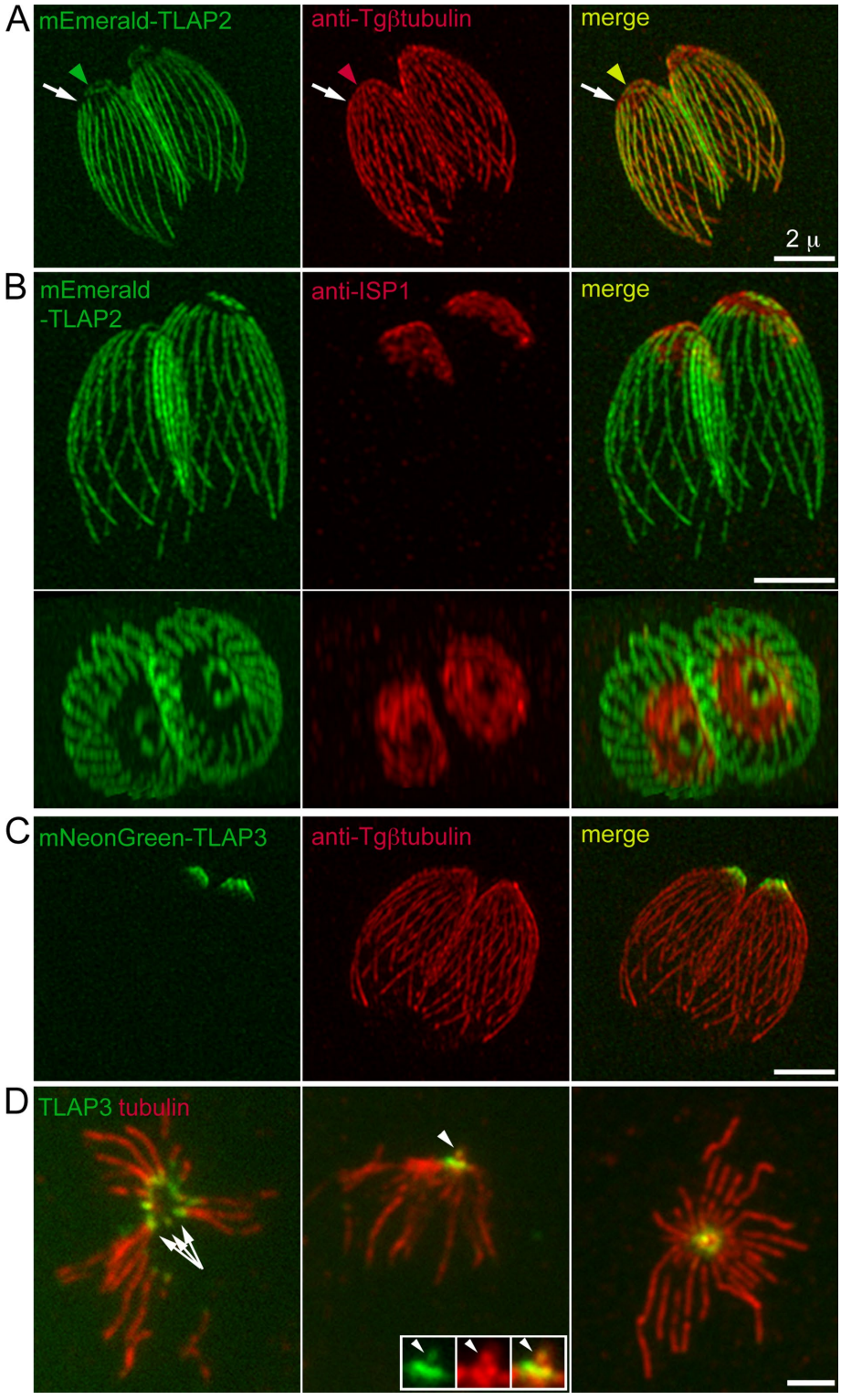


FIGURE 2: TLAP2 and TLAP3 associate with distinct sections of the cortical microtubules. (A) 3D-SIM projections of intracellular *mEmeraldFP-TLAP2* knock-in parasites labeled with a rabbit anti–Tgβ-tubulin antibody (Morrissette and Sibley, 2002b), indicating that TLAP2 decorates the microtubules in a segmental manner. TLAP2 is present in a ring-like structure (arrowheads) and absent from an apical portion of the cortical microtubules (arrows) and coats the rest of the polymers distal to the gap. Note that under this condition, the antibody does not label the conoid, likely due to poor antigen accessibility (Supplemental Figure S1A). To correct for lateral chromatic aberration, the image for the anti-tubulin channel was digitally magnified by 1.01× and left-shifted by 1 pixel (~40 nm). Green, mEmeraldFP-TLAP2. Red, anti–Tgβ-tubulin. Scale bar, 2 μm. (B) 3D-SIM projections that give side (top) and top (bottom) views of a pair of intracellular *mEmeraldFP-TLAP2* knock-in parasites labeled with a mouse anti-ISP1 antibody (see also Supplemental Video S1). The apical region free of TLAP2 partially coincides with a "cap" marked by ISP1, a protein inserted into the apical portion of the IMC through a lipid anchor (Beck *et al.*, 2010). Green, mEmeraldFP-TLAP2. Red, anti-ISP1. Scale bar, 2 μm. (C) 3D-SIM projections of intracellular *mNeonGreenFP-TLAP3* knock-in parasites labeled with a rabbit anti–Tgβ-tubulin antibody, showing that TLAP3 is located to an anterior portion of the parasite. Green, mNeonGreenFP-TLAP3. Red, anti–Tgβ-tubulin. Scale bar, 2 μm. (D) Wide-field images of mouse anti–α- and β-tubulin antibody labeling of extracellular *mNeonGreenFP-TLAP3* knock-in parasites extracted with Triton X-100 (left), followed by fixation with 3.7% (vol/vol) formaldehyde or extracted with 0.5% (wt/vol) sodium deoxycholate, followed by fixation with formaldehyde (middle) or methanol (right), showing that TLAP3 is localized to the apical section of the cortical microtubules (arrows), as well as intraconoid microtubules (arrowheads). Green, mNeonGreenFP-TLAP3. Red, anti-tubulin. Scale bar, 2 μm. Inset, 1.5×.

mitotic spindle are both highlighted by another protein found in our previous proteomic screen (Liu *et al.*, 2013), TLAP4 (TGGT1_201760; EuPathDB.org), tagged with a fluorescent protein and ectopically expressed from a *T. gondii* tubulin promoter (Hu *et al.*, 2002b). In these parasites, a number of other cytoskeletal structures were also highlighted by various fluorescently tagged markers, including TgCentrin1 for highlighting the centrioles (Figure 4D), TLAP3 for highlighting the apical section of cortical microtubules (Figure 4E), and MORN1 for labeling the basal complex, a protein complex located at the extreme basal end of the parasite (Figure 4F; see also Figure 1; Hu *et al.*, 2006; Hu, 2008; Heaslip *et al.*, 2010). The signal of fluorescently tagged TLAP4 in the spindle first appears in a spot adjacent to centrioles (Figure 4, A–D, panel 1). By the time the nascent daughters, shaped like a flattened disk, are built around the centrioles, the bar shape of the spindle in the nucleus has become apparent, with the centrioles close to but distinctly separated from the spindle poles (Figure 4D, panel 2). The daughter cytoskeleton is fully polarized at an early stage, as indicated by the construction of the TLAP3 "cap" and the basal complex, structures corresponding to the apical and basal portions of the future parasites, respectively (Figure 4, E and F, panel 2). Similar to what is shown in Figure 3A, TLAP3 is present in a cluster of

dots in nascent daughter parasites (Figure 4E, panel 2) but not in the mitotic spindle. Of interest, fluorescently tagged TLAP4 labeling in the daughters is similarly arranged but extends more distally, indicating differential decoration of the cortical microtubules in the daughters (Figure 4E, insets). As the daughters grow, the TLAP4 labeling of the spindle further shortens (Figure 4, B and D–F, panel 4), the TLAP3 labeling persists at the apical region (Figure 4E, panel 4), and the ring-shaped basal complex remains abutting the basal end of the daughters (Figure 4F, panel 4).

How is the specific localization of a coating protein achieved? TLAP3 is recruited to the apical region of the cortical microtubules during daughter construction. A simple hypothesis is that this region contains TLAP3-specific binding sites that are not available on the rest of the cortical microtubules or mitotic spindle. However, we found this not to be the case. When fluorescently tagged TLAP3 is ectopically expressed from a *T. gondii* tubulin promoter, it is localized to the full length of the cortical microtubules and nascent spindle (Figure 5), indicating that TLAP3 binding sites are not limited to the apical region of the microtubule cytoskeleton. An alternative hypothesis is that the native expression of TLAP3 is modulated such that the protein is available only when the apical section of cortical microtubules is forming. To generate specific targeting in this scenario, TLAP3 needs to associate irreversibly with the polymer once bound. Otherwise, protein molecules associated with the sections of microtubules built earlier would be able to dissociate and bind to the newly grown portion and result in coating the entire length of the microtubule. To test the reversibility of TLAP3 binding, we performed fluorescence recovery after photobleaching (FRAP) experiments. Figure 6A and Supplemental Video S3 show a vacuole containing two *mNeonGreenFP-TLAP3* knock-in parasites in which daughter parasites had formed before the photobleaching. The mNeonGreenFP-TLAP3 cap was bleached in one of the mothers (cyan arrow) and one of its nascent daughters (magenta arrow). During the postbleach period, mNeonGreenFP-TLAP3 was incorporated into the cap region of the bleached daughter but not the mother, indicating that newly synthesized mNeonGreenFP-TLAP3 is specifically targeted to growing daughters but not the mother. Of importance, the difference in intensity between the bleached and unbleached daughter parasites (Figure 6A, magenta and red lines in graph) was maintained through daughter construction and budding, indicating that, once bound, TLAP3 indeed does not dissociate from the daughter cytoskeleton. We next tested whether the availability of TLAP3 is coupled with the polymerization of cortical microtubules in the cap region by examining the timing of TLAP3 recruitment with respect to the growth of cortical microtubules in daughters. FRAP and time-lapse imaging in *mNeonGreenFP-TLAP3* knock-in parasites expressing mCherryFP-Tgα1-tubulin show that the incorporation of TLAP3 continues after the microtubules grow past the TLAP3 cap (Figure 6B, time points 0:19:47; 0:29:48, and 0:39:47; magenta and green lines in graph). This indicates that specific targeting to the cap region in daughter parasites is not entirely controlled by the time window within which mNeonGreenFP-TLAP3 is available. Thus additional factors besides the TLAP3 protein itself and regulation of protein expression constitute the "code" for specific targeting.

### The coating proteins show different microtubule-binding properties

The coating proteins described here are localized to an array of microtubule-containing structures or subregions within these structures. Do they interact with microtubules directly or via adaptor proteins? We reasoned that although some coating proteins might require parasite-specific factors to bind to microtubules in *T. gondii*, if a coating protein is able to associate with microtubules in a foreign environment devoid of other parasite proteins, then its binding to the polymer is more likely to be direct. We thus first expressed mEmeraldFP-tagged proteins in human foreskin fibroblast (HFF) cells and tested whether they colocalize with the microtubules. Of all the *T. gondii* microtubule-coating proteins tested, only mEmeraldFP-TLAP2 labels microtubule-like fibers in HFF cells (Figure 7A). Expression of these fluorescently tagged proteins in other mammalian cell lines gave similar results (unpublished data). To further confirm that these fibers are formed of microtubules, we expressed mEmeraldFP-TLAP2 in a transgenic HeLa cell line stably expressing mCherryFP-tubulin and found that the mEmeraldFP-TLAP2-labeled fibers colocalize with a subpopulation of mCherryFP-labeled microtubules in transfected cells (Figure 7B). Moreover, TLAP2 often bundles microtubules, indicated by the higher intensity of mCherryFP-tubulin in the TLAP2-containing fibers (Figure 7B). Of interest, the TLAP2 coating on the microtubules is dense enough to block access to the epitopes recognized by anti α- and β-tubulin monoclonal antibodies used for the immunolabeling (Figure 7C).

To determine whether TLAP2 is capable of bundling microtubules on its own, we purified recombinant FLAG-TLAP2 protein expressed in *Escherichia coli* (Figure 7D) and incubated the purified protein with in vitro–polymerized microtubules. We analyzed the mixture using dark-field microscopy, in which bundled microtubules generate much brighter signal than single microtubules due to more efficient light scattering. The microtubules were indeed bundled after incubation with recombinant FLAG-TLAP2 compared with the control (Figure 7E). Microtubule bundling occurred within 5 min, that is, the typical time it took to set up the reaction, load the sample into a slide chamber, and bring it to focus on the microscope to begin imaging.

The potent microtubule-bundling activity of TLAP2 in vitro and in mammalian cells predicts that its overexpression in *T. gondii* should alter the kinetics of microtubule polymerization in the parasite and would therefore be a useful tool to probe microtubule organization and function in *T. gondii.* Indeed, ectopic expression of TLAP2 driven by a tubulin promoter induces changes in the organization of the parasite microtubule cytoskeleton. There are several informative patterns. Figure 8, A and B, shows single transgenic parasites expressing enhanced green fluorescent protein (eGFP)–Tgβ2–tubulin (pseudocolored red) in which transiently expressed mAppleFP-TLAP2 (pseudocolored green) appeared to promote elongation of the preexisting cortical microtubules. Many microtubules extended from the apical to the basal end of the parasite instead of terminating at approximately two-thirds of the parasite body. The decoration of mAppleFP-TLAP2 on these microtubules was more prominent on the distal segments (arrows), likely due to exclusion by endogenous coating proteins already associating with cortical microtubules before the ectopic expression of mAppleFP-TLAP2. Consistent with in vitro observations, some TLAP2-decorated microtubules coalesce to form bundles (Figure 8B, insets). A higher level of TLAP2 expression results in grossly misshapen parasites in which the organization of the microtubule cytoskeleton is completely altered (Figure 8C). These parasites can grow to a size comparable to that of a multiparasite vacuole, as shown in Figure 8D, a ~14 µm × 16 µm parasite mass. In this example, the IMC labeling highlighted irregular extensions close to the periphery of the parasite. The morphology of some of the extensions suggests aberrant daughter formation and budding (Figure 8D, inset). We conclude that a balanced expression of coating proteins is critical to generate and maintain the organization, as well as to control the length, of the cortical microtubules.

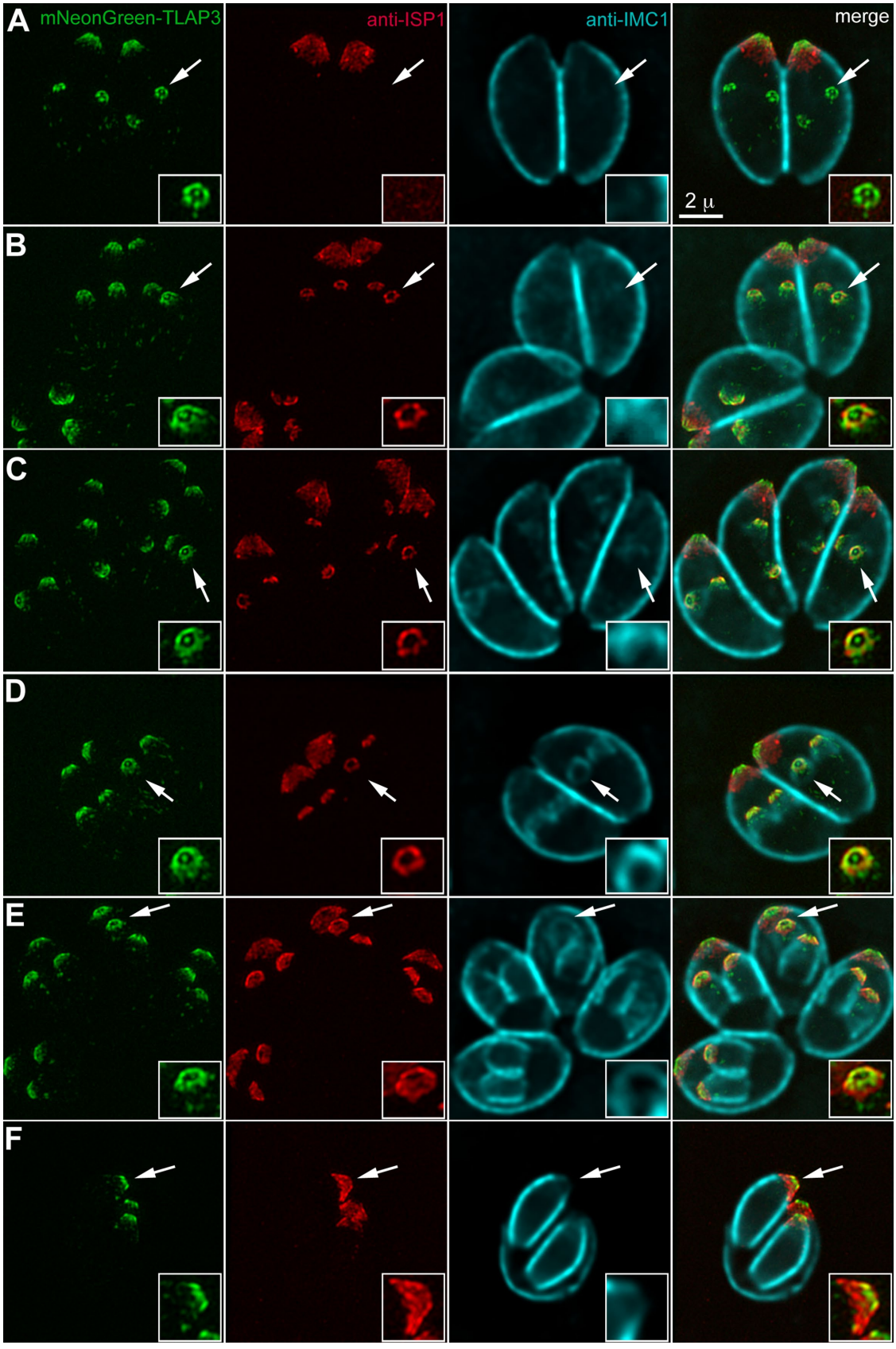


FIGURE 3: TLAP3 decoration of the cortical microtubules is established early during daughter construction. (A–F) *mNeonGreenFP-TLAP3* knock-in parasites at different stages of the cell cycle labeled with a mouse anti-ISP1 antibody and a rabbit anti-IMC1 antibody. The mNeonGreenFP-TLAP3 and anti-ISP1 images are projections of 3D-SIM images. The anti-IMC1 images, visualized by a goat anti-rabbit Cy5 antibody, are projections of deconvolved wide-field

### Extensive functional redundancy among the coating proteins

TLAP2 is conserved among several distinct groups of apicomplexans, including *Plasmodium* spp. and close relatives of *Toxoplasma* in the subclass Coccidia, estimated to have diverged several hundred million years ago (Escalante and Ayala, 1995; Douzery *et al.*, 2004; Kuo *et al.*, 2008). Of interest, a TLAP2 homologue is also found in *Chromera velia*, a photosynthetic distant relative of the apicomplexans, indicating that TLAP2 was present in the common ancestor of parasitic apicomplexans and free-living *C. velia* (Figure 9A and Supplemental Figure S2). However, no significant homologue of TLAP2 is found in the predicted protein databases for subclasses cryptosporidia, gregarines, or piroplasms by BLASTP (*E*-value cut-off 0.005), suggesting that the gene might have been lost in these groups after their common ancestor diverged from that of coccidians and the *Plasmodium* spp. The conserved portion of TLAP2 homologues lies within the C-terminal ~200 amino acids, which contain an unusually high number of conserved tryptophan residues. Two TLAP2 homologues are found in *Plasmodium falciparum*, which we named PfTLAP2-a (PF3D7_1034300; EuPathDB.org) and PfTLAP2-b (PF3D7_0517200), with PfTLAP2-a sharing a higher degree of similarity with TgTLAP2 (Figure 9A). Of the 14 tryptophan residues in the C-terminal domain of TgTLAP2, nine are conserved in both PfTLAP2-a and CvTLAP2 (Figure 9A). Consistent with the high level of conservation in this region, the C-terminal 276 amino acids (aa) of TgTLAP2 are sufficient to induce the formation of bundles when expressed in *T. gondii* (Supplemental Figure S2). The N-terminal sequences of TLAP2 in *T. gondii* and *Plasmodium* spp. are both of low complexity and not conserved. The N-terminal 2–180 aa of TgTLAP2 are cytosolic when ectopically expressed and tagged with mEmeraldFP (Supplemental Figure S2). To test whether PfTLAP2-a potentially associates with microtubules, we transiently expressed mEmeraldFP-PfTLAP2-a from a tubulin promoter in *T. gondii* and often observed that mEmeraldFP-PfTLAP2-a concentrated at the apical portion of the cortex in mature parasites (Figure 9B) and two internal clusters with six or seven spots reminiscent of TLAP3 labeling of nascent daughter parasites (Figure 9B, top). In some other cases, surface stripes similar to cortical microtubules were seen (Figure 9B, bottom). These results suggest that PfTLAP2-a might also be able to associate with cortical microtubules.

The conservation of TLAP2 among distant apicomplexan lineages, its ability to bind directly to and bundle microtubules, and its dominant effect on the organization of the microtubule cytoskeleton when ectopically expressed all suggest that TLAP2 is functionally important for the parasites. We thus generated a TLAP2-knockout *T. gondii* (Δ*tlap2*), using an established recombination method based on a Cre-LoxP strategy (Heaslip *et al.*, 2010, 2011; Liu *et al.*, 2013). After transiently expressing Cre recombinase in *mEmeraldFP-TLAP2* knock-in parasites, we excised the LoxP-flanked cassette containing the coding sequence for mEmeraldFP-TLAP2 in transfected parasites (Figure 9C). We then selected Δ*tlap2* clones from a mixed population by fluorescence-activated cell sorting (FACS) based on the loss of mEmeraldFP fluorescence (Figure 9, C and D, and Supplemental Figure S3A). Surprisingly, Δ*tlap2* parasites did not have an obvious growth defect. After growth in a confluent monolayer of host cells for 7 d at 37°C, Δ*tlap2* parasites formed a comparable number and size of plaques as the parental RHΔ*hx* and *mEmeraldFP-TLAP2* knock-in parasite lines (Supplemental Figure S3B; number of plaques = 103% of RHΔ*hx*, $n = 4$, SD = 5%). Furthermore, infection of mice showed that Δ*tlap2* parasites did not exhibit a significant loss of virulence (Figure 9E). Mice infected with the RHΔ*hx* parasites died between days 7 and 8 postinfection, whereas the mice infected with the *mEmeraldFP-TLAP2* knock-in and Δ*tlap2* parasites died between days 8 and 9 postinfection. This suggests that the loss of *tlap2* is compensated for by other factors, such as other microtubule-coating protein(s). Minor fitness defects were also observed in the knockout mutants of two other coating proteins, SPM1 and TrxL1 (Tran *et al.*, 2012; Liu *et al.*, 2013), which again suggests functional redundancy among the coating proteins. Consistent with this idea, we found that these coating proteins associate with the cortical microtubules through independent mechanisms. Fluorescently tagged SPM1, and TLAPs 1, 3, and 4 were localized to the cortical microtubules when expressed in Δ*tlap2* parasites (Figure 9F, top, and Supplemental Figure S3C), indicating that the association of these proteins with the polymers is not dependent on TLAP2. Similarly, in the absence of SPM1, TLAP2 and TLAP3 are able to associate with the cortical microtubules (Figure 9F, bottom). To test directly the functional redundancy among the coating proteins, we used the Cre-LoxP strategy to generate a panel of new knockout mutants (Supplemental Figures S4 and S5)—Δ*tlap3*, Δ*tlap2*Δ*spm1*, and Δ*tlap2*Δ*spm1*Δ*tlap3* parasites—and examined their growth. Δ*tlap3* parasites did not display a notable growth defect (Supplemental Figure S4). Even the Δ*tlap2*Δ*spm1* double-knockout parasites grew robustly (number of plaques = 79% of RHΔ*hx* control, $n = 4$, SD = 4%; Figure 9G). However, the Δ*tlap2*Δ*spm1*Δ*tlap3* triple-knockout mutant showed a pronounced fitness effect, generating fewer plaques than the parental parasites under the same condition (number of plaques = 24% of RHΔ*hx* control, $n = 3$, SD = 21%; Figure 9G).

### The coating proteins protect the stability of cortical microtubules as an ensemble

One of the most remarkable features of the cortical microtubules in *T. gondii* is that they are extraordinarily stable; thus the reduced fitness in Δ*tlap2*Δ*spm1*Δ*tlap3* parasites could be due to changes in the organization or integrity of the cortical microtubules. To determine whether the loss of coating proteins affects the stability of cortical microtubules, we used cold-temperature treatment, which has been widely used in studies of stability control of the microtubule cytoskeleton in animal and plant cells (Salmon and Begg, 1980; Jasmin *et al.*, 1990; Detrich *et al.*, 2000; Abdrakhamanova *et al.*, 2003; Zhu *et al.*, 2006; De Storme *et al.*, 2012; Oropesa-Avila *et al.*, 2014). We compared microtubule stability in cold conditions (8°C) for the Δ*tlap2*, Δ*spm1* (Tran *et al.*, 2012), Δ*tlap3*, Δ*tlap2*Δ*spm1*, and Δ*tlap2*Δ*spm1*Δ*tlap3* parasites, using a rabbit anti–Tgβ-tubulin antibody (Morrissette and Sibley, 2002b) to specifically label *T. gondii* but not host cell microtubules. The cortical microtubules in the parental line (RHΔ*hx*) remained stable after incubation at 8°C for 3.5 h followed by the procedure of immunolabeling (Figure 10A). In Δ*tlap2*, Δ*spm1*, and Δ*tlap3* single-knockout mutants, the cortical

images, as the Cy5 fluorophore is not compatible with SIM imaging. Surface sections were not included in the anti-IMC1 projections to better display the signal from daughter cells. The Cy5 channel was misregistered slightly with the other two channels. Alignment was done by manually lining up the edge of ISP1 and IMC1 labeling. Insets (2×) are contrast enhanced and include regions of daughter parasites indicated by the arrows. For clarity, the IMC1 channel is not shown in the insets of the merged image panels. Green, mNeonGreenFP-TLAP3. Red, anti-ISP1. Cyan, anti-IMC1. Scale bars, 2 μm.

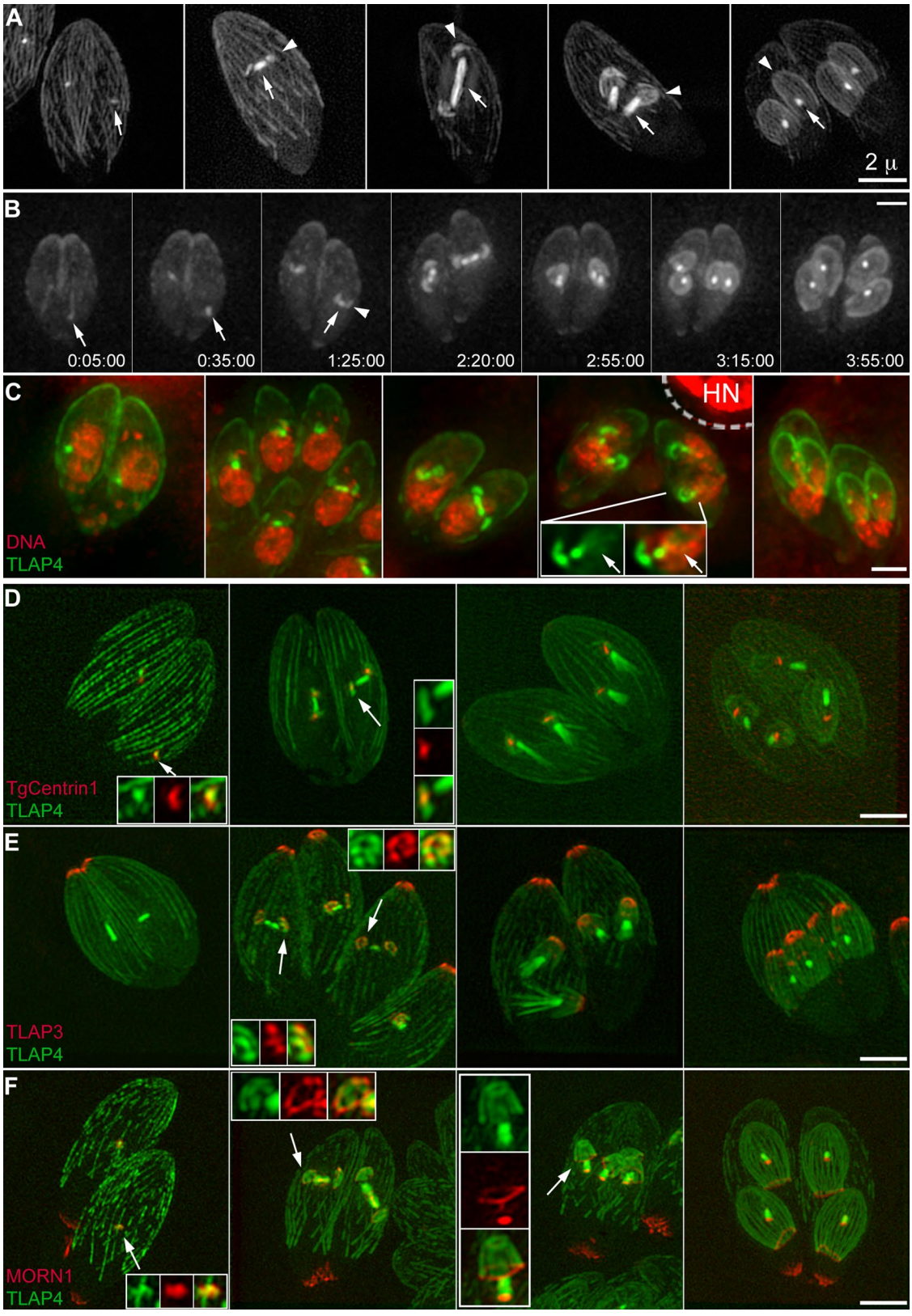


FIGURE 4: Assembly of the mitotic spindle during daughter construction as visualized by ectopic expression of mEmeraldFP-TLAP4 driven by a *T. gondii* tubulin promoter. (A) 3D-SIM projections of five different vacuoles containing *ptub-mEmeraldFP-TLAP4* transgenic parasites, ordered according to the stage of daughter assembly (arrowheads). In interphase parasites, mEmeraldFP-TLAP4 mostly resides on the cortical microtubules (panel 1). After construction of the daughter cytoskeleton is initiated, the TLAP4 signal in the spindle (arrows) becomes much more intense than that of the cortical microtubules in the mother parasite (panels 2–5). Depending on the orientation of the spindle axis with respect to that of the parasite, the length of the spindle can reach as long as ~2 μm. Scale bar, 2 μm. (B) Selected panels from a

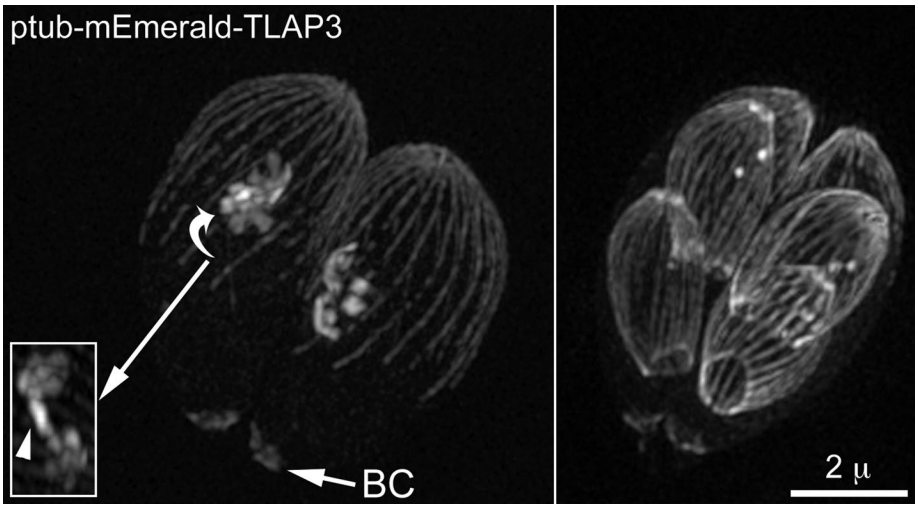


FIGURE 5: Replicating parasites ectopically expressing mEmeraldFP-TLAP3 from a *T. gondii* tubulin promoter. Each panel shows a vacuole containing two intracellular parasites with nascent daughters (left) or close-to-budding daughters (right). Note that when overexpressed, TLAP3 is capable of coating the full length of the cortical microtubules, as well as of localizing to the basal complex (BC) and nascent spindle (inset, arrowhead). The inset (1×) shows a different rotational view of the region indicated by the arrow.

microtubules were also clearly labeled by the tubulin antibody. In contrast, in interphase Δ*tlap2*Δ*spm1* parasites, the anti–Tgβ-tubulin labeling was reduced to a cap in the apical region (Figure 10A), reminiscent of the region occupied by TLAP3 (Figure 2). Indeed, this apical labeling was further reduced to a small, ring-like structure with the additional loss of TLAP3 (Figure 10A, Δ*tlap2*Δ*spm1*Δ*tlap3*) and could be restored by mNeonGreenFP-TLAP3 expression (Figure 10A, Δ*tlap2*Δ*spm1*Δ*tlap3*-TLAP3 rescue). Even without cold treatment, instability of the cortical microtubules in Δ*tlap2*Δ*spm1* and Δ*tlap2*Δ*spm1*Δ*tlap3* parasites was already pronounced, although the extent of destabilization was more variable (Figure 10B). Of interest, we found that in dividing Δ*tlap2*Δ*spm1* or Δ*tlap2*Δ*spm1*Δ*tlap3* parasites, whereas cortical microtubules of the mother appeared to be much shorter than those in the parental strain (Figure 10C), the anti–Tgβ-tubulin labeling of the mitotic spindle (Figure 10C, columns 3 and 5) and cortical microtubules of daughters (Figure 10C, columns 4 and 6) remained prominent, although we could not determine whether all cortical microtubules are present in the daughters, due to an inadequate signal-to-background ratio in the data. This differential sensitivity suggests that unique coating proteins or modifications confer additional protection to microtubules in daughters. Alternatively, the cortical microtubules in an adult parasite might undergo further modifications that reduce the protection against depolymerization.

## DISCUSSION

### Specific targeting of associated proteins to microtubules

The specific localization of proteins allows for functional differentiation within a cell. It has been established that the specificity in protein targeting to different membrane-bound organelles is mainly achieved by the match between the cargo and receptors that recognize the signal encoded in the cargo and guide it to its destination. In contrast, the mechanics that governs specific targeting to subregions or subsets of cytoskeletal polymers is considerably less well understood. There are many functionally distinct microtubule-based structures in eukaryotic cells, including the interphase microtubule array, centrioles, flagellum/cilium, and mitotic spindle. Each of these structures has its own unique set of associated proteins with distinct localization. For instance, the tumor suppressor Ras association domain–family protein 1A preferentially associates with perinuclear microtubules (Arnette *et al.*, 2014). In neurons, the microtubules in dendrites and axons are differentially decorated with MAP2 and tau (Caceres *et al.*, 1984; Binder *et al.*, 1985; Papasozomenos *et al.*, 1985). Unlike the membrane of organelles, microtubules are formed of large (8 nm), periodically repeating units. Aside

time-lapse movie of *ptub-mEmeraldFP-TLAP4* transgenic parasites after the construction of the mitotic spindle and cortical microtubules of daughters (also see Supplemental Video S2). The mitotic spindle originates from a spot (arrows) located close to the base of the nucleus at the beginning of this experiment. The assembly of daughters (arrowhead) is initiated close to the poles of the spindle and continues after the TLAP4 signal in the spindle shortens. The later phase of spindle and daughter assembly occurs close to the side of nucleus facing the apical end of the cell. Scale bar, 2 μm. (C) Projections of deconvolved wide-field images of five different vacuoles containing *ptub-mEmeraldFP-TLAP4* transgenic parasites labeled with Hoechst 33342 (pseudocolored red) ordered according to the stage of daughter assembly. The inset (1.5×) shows a daughter parasite adjacent to a half-spindle resembling a comet tail (arrows). Green, mEmeraldFP-TLAP4. Red, DNA staining by Hoechst 33342. HN, host cell nucleus. The region within the dashed line was excluded in adjustment for brightness and contrast for the Hoechst 33342 channel due to the strong signal from the host cell nucleus. Scale bar, 2 μm. (D) 3D-SIM projections of parasites ectopically expressing mAppleFP-TLAP4 and mEmeraldFP-TgCentrin1, which labels the centrioles. Insets (2.4×) include regions indicated by the arrows. Green, mAppleFP-TLAP4. Red, mEmeraldFP-TgCentrin1. Scale bar, 2 μm. (E) 3D-SIM projections of *mNeonGreenFP-TLAP3* knock-in parasites ectopically expressing mAppleFP-TLAP4. Insets (2.4×) include regions indicated by the arrows. Green, mAppleFP-TLAP4. Red, mNeonGreenFP-TLAP3. Scale bar, 2 μm. (F) 3D-SIM projections of *ptub-mEmeraldFP-TLAP4* transgenic parasites ectopically expressing mTagRFP-MORN1. mTagRFP-MORN1 marks the basal complex, which is assembled at an early stage (panel 2; also see Figure 1). In addition to the basal complexes of both daughters and the mother, mTagRFP-MORN1 is also localized to two spots, consistently basal to the concentrated mEmeraldFP-TLAP4 signal at the poles (panels 3 and 4). As the daughters grow, the ring-shaped basal complex continues to abut the basal end of the daughters (panel 4). In fully matured parasites, the distal tips of the cortical microtubules are separated from the basal complex by an ~1- to 2-μm gap, and the mTagRFP-MORN1 labeling at the spindle pole persists (panel 1, inset). Insets (2× for panel 3 and 2.4× for all others) include regions indicated by the arrows. Green, mEmeraldFP-TLAP4. Red, mTagRFP-MORN1. Scale bar, 2 μm.

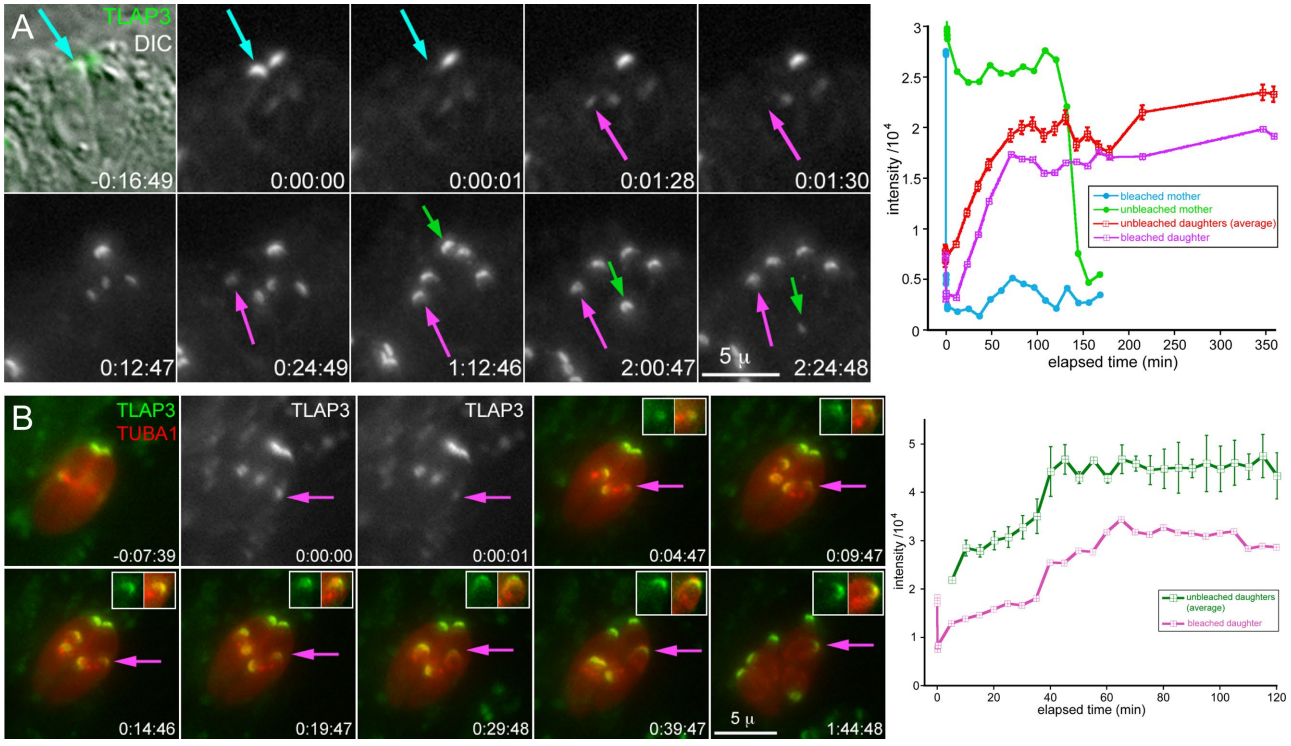


FIGURE 6: FRAP of *mNeonGreenFP-TLAP3* knock-in parasites. (A) Selected images showing a vacuole containing two *mNeonGreenFP-TLAP3* knock-in parasites in which nascent daughter parasites had formed before the photobleaching (also see Supplemental Video S3). The mNeonGreenFP-TLAP3 cap was bleached in one of the mothers (cyan arrow, 0:00:01) and one of its nascent daughter parasites (magenta arrow, 0:01:30). The green arrow indicates the unbleached mother transported to the base of the vacuole and degraded as the daughters completed budding. The graph on the right shows the intensity measurements of mNeonGreenFP-TLAP3 in the cap region of the bleached mother (cyan), unbleached mother (green), and bleached daughter (magenta) and the average for unbleached daughters (red). *X*-axis, elapsed time (minutes). *Y*-axis, measured intensity/$10^4$. Error bars are ±SEM. (B) Selected images showing a vacuole containing two *mNeonGreenFP-TLAP3* knock-in parasites expressing mCherryFP-Tgα1-tubulin (TUBA1). Nascent daughter parasites had formed before the photobleaching. The mNeonGreenFP-TLAP3 cap was partially bleached in one of the nascent daughter parasites (magenta arrow, 0:00:01). Insets: 1.25×. The graph on the right shows the intensity measurements of mNeonGreenFP-TLAP3 in the cap region of the bleached daughter (magenta) and the average for unbleached daughters (green). *X*-axis: elapsed time (minutes). *Y*-axis: measured intensity/$10^4$. Error bars are ±SEM.

from the two ends of the polymer, the core structure of one section of a microtubule is virtually indistinguishable from any other; therefore, there is no inherent "address" information. Although posttranslational modifications of tubulins have been correlated with the "age" of microtubules and implicated in fine-tuning the interaction between certain motor proteins and the polymer (Bulinski *et al.*, 1988; Stephens, 1992; Luduena, 1998; Kreitzer *et al.*, 1999; Rosenbaum, 2000; Westermann and Weber, 2003; Konishi and Setou, 2009; Janke and Kneussel, 2010; Barisic *et al.*, 2015), it is unclear whether this is a general mechanism that dictates the localization of microtubule-associated proteins or vice versa.

*T. gondii* is a powerful system for understanding how specific targeting to cytoskeletal polymers is achieved, since the pattern of decoration on cortical microtubules is not only defined but also is reproducible from cell to cell and generation to generation (Figures 2 and 3). Furthermore, during replication, daughter microtubules are made de novo, whereas those of the mother remain present. Thus old and new microtubules coexist in the same cell and are readily distinguishable from each other. The tractability of this system makes it possible to delineate biophysical constraints for the biogenesis of a new set of cytoskeletal structures. In this work, we show that daughter cortical microtubules are differentially coated with associated proteins from a very early stage (Figure 3). Of interest, the mechanism for specific targeting appears to be complex even for the seemingly simple localization pattern of TLAP3, a protein targeted to a short apical section of the cortical microtubules. Because TLAP3 is capable of associating with the full length of cortical microtubules when ectopically expressed from a constitutive promoter (Figure 5), the binding sites for TLAP3 cannot be limited to the apical section of the cortical microtubules. This also indicates that the localization of a coating protein can be affected by the timing and level of its expression. However, modulation of protein expression alone cannot explain the specific targeting of TLAP3, because in the *mNeonGreenFP-TLAP3* knock-in parasites, although mNeonGreenFP-TLAP3 irreversibly "paints" the forming cortical microtubules in daughters from an early stage (Figures 3 and 6), it continues to be incorporated into the apical region after the microtubules have extended beyond the region (Figure 6B). In other words, TLAP3 is somehow prevented from binding to the section distal to the cap region. It is possible that, when expressed from the native promoter, TLAP3 is competed off by other coating proteins associating with the distal section, but this competition can be

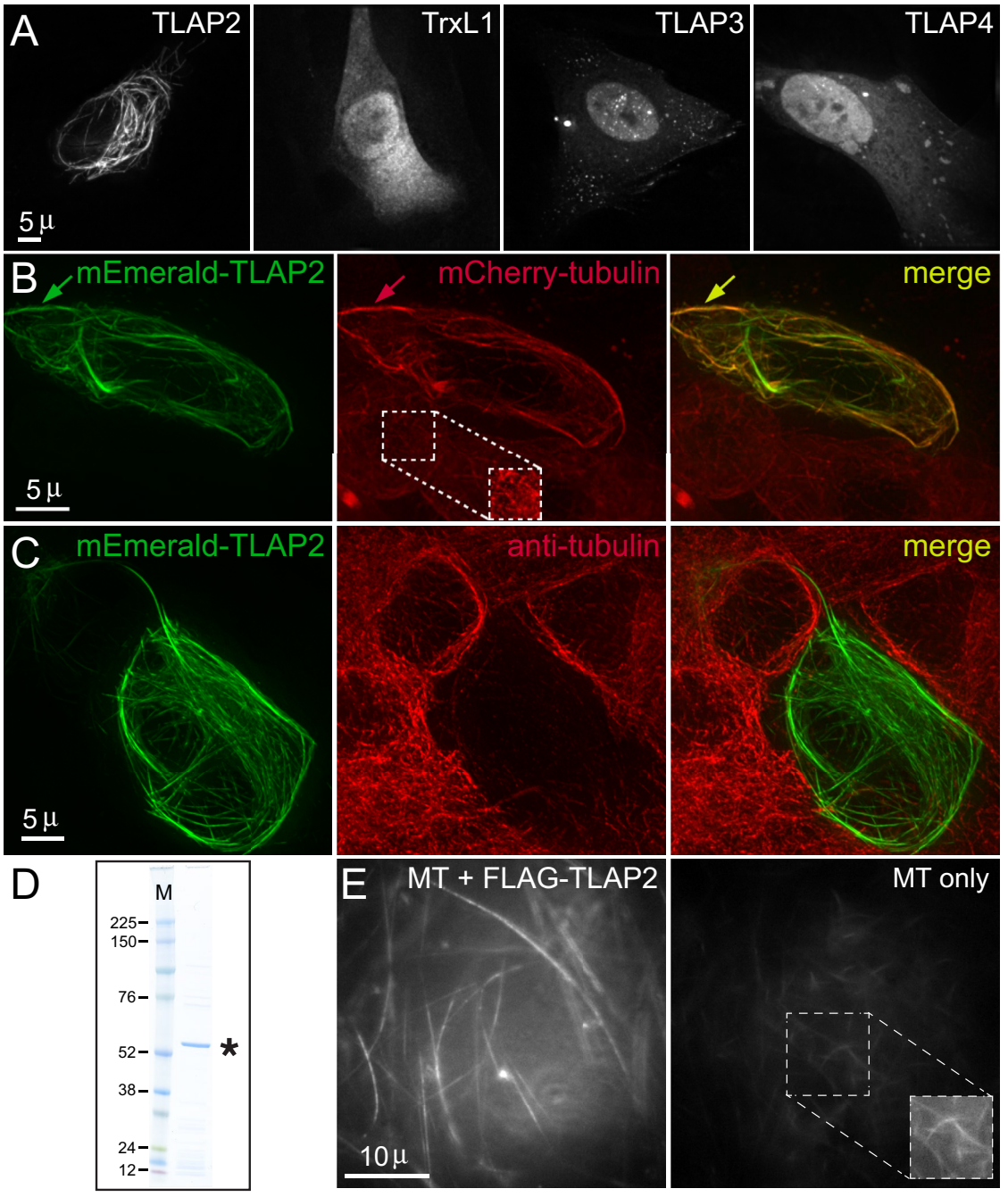


FIGURE 7: The coating proteins display different microtubule-binding properties. (A) Deconvolved wide-field images of HFF cells expressing mEmeraldFP-tagged TLAP2, TrxL1, TLAP3, or TLAP4, showing that only mEmeraldFP-TLAP2 is localized to microtubule-like fibers. (B) Deconvolved wide-field images of a HeLa cell line stably expressing mCherryFP-tubulin (red) transfected with a plasmid expressing mEmeraldFP-TLAP2. Arrows indicate an mEmeraldFP-TLAP2–containing bundle in which the mCherryFP-tubulin signal is much stronger than that in adjacent, untransfected cells. This cell line also stably expresses eGFP-Histone2B, not seen in the image because the eGFP-Histone2B signal is much weaker than that of mEmeraldFP-TLAP2. The inset (1×) in the middle panel is contrast enhanced to display the mCherryFP-tubulin signal in an adjacent, untransfected cell. Green, mEmeraldFP-TLAP2. Red, mCherryFP-tubulin. (C) Deconvolved wide-field images of mEmeraldFP-TLAP2 (green) expression in Vero cells labeled with mouse anti–α- and β-tubulin antibodies (red), showing that the tubulin antibody labeling in a cell expressing mEmeraldFP-TLAP2 is dramatically attenuated compared with untransfected cells, likely due to the blockage of epitopes in the microtubules by the mEmeraldFP-TLAP2 coating. Green, mEmeraldFP-TLAP2. Red, anti-tubulin. (D) SDS–PAGE analysis of a preparation of recombinant FLAG-TLAP2 protein (asterisk) purified from bacterial lysate. The gel was stained by colloidal Coomassie blue. M, molecular weight marker (kilodaltons). (E) Dark-field images of in vitro–polymerized microtubules equivalent to 0.5 µM total tubulin dimer incubated with 0.25 µM purified FLAG-TLAP2 protein (left) or buffer control (right). The conditions for acquisition and display are identical for the two images. The inset (1×) in the right panel is contrast enhanced to display the weak signal in the control reaction.

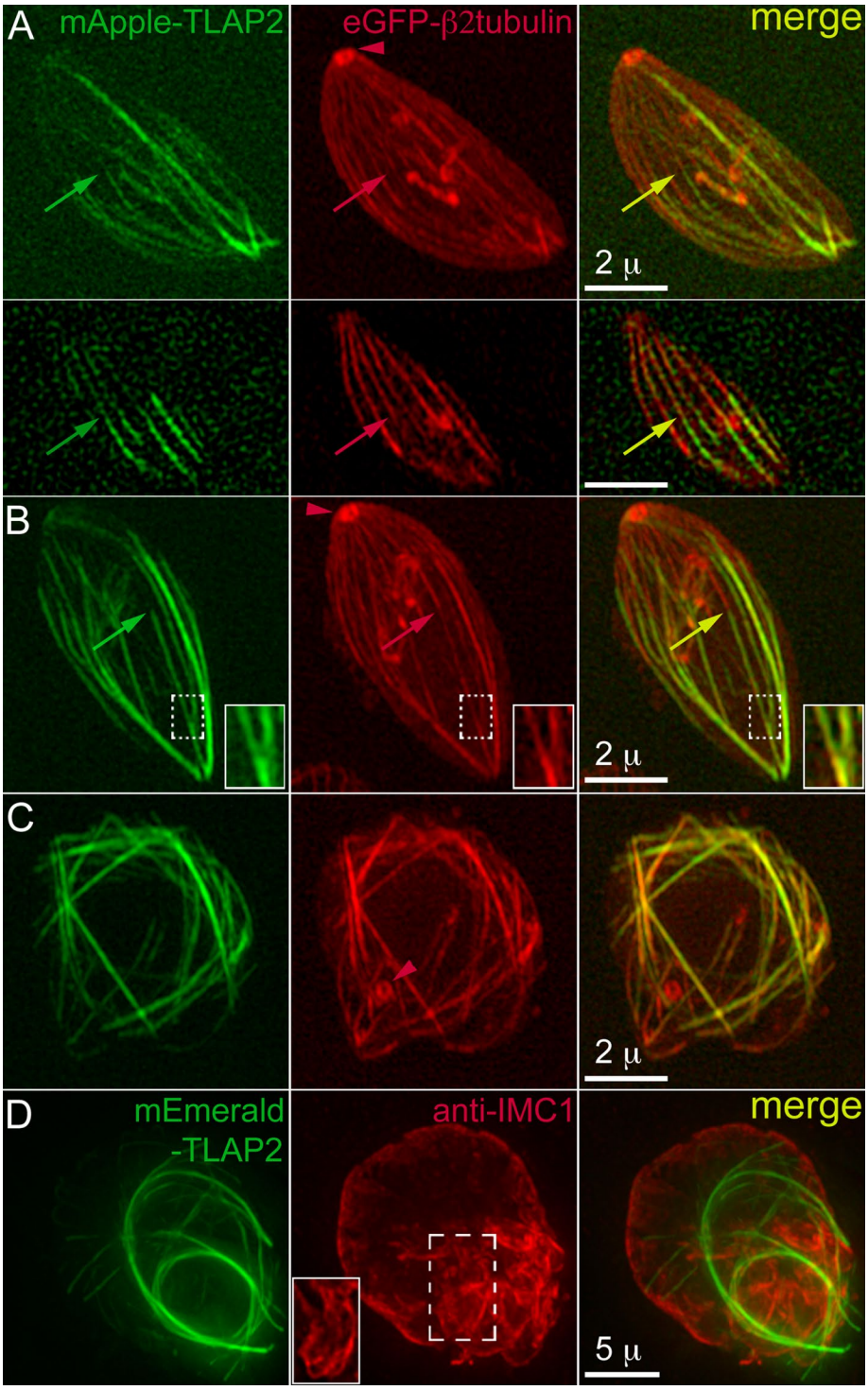


FIGURE 8: Ectopic expression of fluorescently tagged TLAP2 from a tubulin promoter induces the formation of microtubule bundles in *T. gondii*. (A) 3D-SIM images of a single eGFP–Tgβ2-tubulin (pseudocolored red) transgenic parasite transiently expressing mAppleFP-TLAP2 (pseudocolored green). Top, projection; bottom, single surface section. Microtubules extend from the apical to the basal end of the parasite instead of terminating at approximately two-thirds as seen in the wild-type parasite. The arrowhead indicates the conoid in the apical complex (see Figure 1). Arrows indicate a microtubule decorated by mAppleFP-TLAP2 prominently at its distal section. Green, mAppleFP-TLAP2. Red, eGFP-Tgβ2-tubulin. Scale bars, 2 μm. (B) Projections of 3D-SIM images of a single eGFP–Tgβ2-tubulin transgenic parasite transiently expressing mAppleFP-TLAP2. As seen in A, some microtubules extend from the apical to the basal end of the parasite and are decorated by mAppleFP-TLAP2 on the distal section (arrows). Some TLAP2-decorated microtubules coalesce to form bundles (insets). The arrowhead indicates the conoid. Insets: 2×. (C) Projections of 3D-SIM images of a mass of eGFP–Tgβ2-tubulin transgenic parasite transiently expressing mAppleFP-TLAP2, in which the organization of the microtubule cytoskeleton and the morphology of the parasite are dramatically altered. The arrowhead indicates the conoid. (D) Projections of deconvolved wide-field images of parasites transiently expressing mEmeraldFP-TLAP2 (green) and labeled with a rabbit anti-IMC1 antibody (red), which marks the cortex of the parasite. Multiple fibers containing mEmeraldFP-TLAP2 form in the cytoplasm, and the shape of the parasite mass (~14 μm × 16 μm) is severely distorted. The anti-IMC1 labeling highlights irregular extensions close to the periphery of the parasite. The inset (1×) shows a surface section in the region indicated by the frame.

overcome by high-level constitutive expression. In the Δ*tlap2*, Δ*spm1*, and Δ*tlap2*Δ*spm1* mutants, TLAP3 is localized to the cap region, indicating that SPM1 and TLAP2 are not the "masking" proteins, if such exist. It also suggests that if the masking mechanism does exist, it is selective and not simply nonspecific crowding. It will be interesting to know what protein(s) or other mechanism(s) restrict the localization of TLAP3, whether the masking is mutual, and what the role of competitive binding is in determining the localization of other coating proteins. In addition to TLAP3, three other coating proteins also decorate cortical microtubules in a segmental pattern: TLAP2 associates with the polymers in two distinct sections (Figure 2), SPM2 associates with the middle section of the polymers (Tran *et al.*, 2012), and a novel kinesin (TGGT1_273560; ToxoDB.org) coats the distal approximately two-thirds of the cortical microtubules (unpublished data). Together these proteins constitute a rich set of probes for exploring the mechanism of specific targeting to microtubules.

Although in the case of TLAP3, the time window of the availability of the coating protein and that for the formation of the region of the polymer to which it binds do not completely overlap, the linear growth of a polymer is still likely to play an important role in establishing differential decoration by the coating proteins, because each section of the polymer can be distinguished from one another simply due to a difference in the timing of construction. This, together with coordinated temporal regulation of the abundance and affinity of coating proteins during polymerization, allows for sophisticated,

differential decoration along the polymer, which in turn provides the structural basis for functional differentiation. The same principle applies if posttranslational modifications of tubulins dictate the interaction between coating proteins and microtubules for differential decoration. In this case, the modifying enzymes need to act during but not after polymerization to establish the initial specific pattern of modification.

### The function of the coating proteins and functional redundancy among them

*T. gondii* has evolved a complex coating on the cortical microtubules in terms of both the decoration pattern and the protein composition. Most of these proteins are found in both the Coccidia subgroup and *Plasmodium* spp., and several (TLAP2, SPM1, TrxL1) are found in members of the phylum Chromerida, photosynthetic relatives of the apicomplexan parasites (Figure 11). This suggests that these microtubule coatings were present early during the evolution of these ancient parasites, and many continue to perform important functions. Our work demonstrates that three of these proteins together, SPM1, TLAP2, and TLAP3, protect the stability of the cortical microtubules in a region-dependent manner. When SPM1 and TLAP2 are both removed, the region of cortical microtubules distal to the TLAP3 cap becomes less stable. The removal of TLAP3 in the Δ*tlap2*Δ*spm1* parasite results in destabilization of microtubules in the apical cap and a significant reduction in parasite fitness. However, elimination of TLAP3 alone does not affect the stability of cortical microtubules, perhaps because SPM1 and TLAP2 play a protective role and prevent depolymerization from occurring at distal ends. It is also possible that SPM1, which coats the entire length of the cortical microtubules, has redundant stabilization effects in the cap region. Under the conditions that cause destabilization of the mother cortical microtubules in the Δ*tlap2*Δ*spm1* and Δ*tlap2*Δ*spm1*Δ*tlap3* mutant parasites, cortical microtubules are still present in the daughters. This suggests that other coating proteins or protective mechanisms remain functional in the microtubule cytoskeleton of the daughters in these genetic backgrounds. Potential candidates include SPM2 (Tran *et al.*, 2012), TLAP1 (Liu *et al.*, 2013), and TLAP4. Although the function of these other coating proteins needs to be explored, mutants generated in this work have opened up new avenues to explore the biogenesis and function of the cortical microtubules. For example, in combination with live probes for microtubules, these mutants will allow us to define precise conditions that destabilize the cortical microtubules in live parasites and address several long-standing questions. Do cortical microtubules, organized into a left-handed spiral, dictate the left-handed helical movement of apicomplexan parasites? Do they maintain the shape of a mature parasite? Our findings also generate new puzzles. For instance, if these coating proteins are simply used to protect the stability of the cortical microtubules, then why does the parasite go to great lengths to generate such an elaborate pattern of segmental decoration? A set of transmembrane proteins in the IMC forms a two-dimensional lattice with a 32-nm longitudinal repeat that is also present in the underlying cortical microtubules, suggesting that these structures are closely coupled (Morrissette *et al.*, 1997). This raises the interesting possibility that segmentation of the protein coat on cortical microtubules dictates that of the membrane cortex. The segmentation of the IMC was first demonstrated structurally in *Eimeria*, a close relative of *T. gondii* (Dubremetz and Torpier, 1978), and then molecularly with the discovery of TgCentrin2 (Hu *et al.*, 2006) and the ISP proteins in *T. gondii* (Beck *et al.*, 2010; Fung *et al.*, 2012). Consistent with the idea that the segmentation of the IMC and the coating of the cortical microtubules might be coupled, we discovered a novel kinesin (TGGT1_273560; ToxoDB.org) that coats the distal section of the cortical microtubules bordering the basal edge of the ISP1 cap (unpublished data). Although the sections of the cortical microtubules that TLAP2 and TLAP3 highlight do not completely align with markers for known IMC subcompartments, it is possible that there are other, unidentified subregions in the IMC. Future ultrastructural studies of mutants lacking one or more coating proteins will be critical to define the influence of the cortical microtubules on the architecture of the membrane cortex.

The extent of functional redundancy among the coating proteins is remarkable. For instance, both TLAP2 and SPM1 are conserved among apicomplexan parasites that diverged several hundred million years ago (Figure 11; Tran *et al.*, 2012). In addition, TLAP2 has a defined and elaborate pattern of localization on the cortical microtubules, displays potent microtubule-bundling activity in vitro, and alters the organization of the microtubule cytoskeleton when heterologously expressed in mammalian cells and ectopically expressed in *T. gondii*. However, each of the coating proteins by itself is fully dispensable for parasite growth. Even a double-knockout mutant of *tlap2* and *spm1* grows robustly, although the cortical microtubules become more susceptible to depolymerization. It is puzzling why *T. gondii* keeps both SPM1 and TLAP2 or why *Plasmodium* spp. maintain two copies of TLAP2 in addition to SPM1. It is possible that these proteins are required for stages of the parasite other than the asexual form examined in this work. For example, both PfTLAP2-a and PfTLAP2-b are most highly transcribed in the ookinete stage (PlasmoDB.org), during which the microtubule cytoskeleton undergoes dramatic reorganization as the parasite develops from a zygote into an oocyst (Aikawa *et al.*, 1984; Kumar *et al.*, 1985). It is also a stage when parasites grow in the mosquito host and might require more stable microtubules, as the environmental temperature is no longer constantly 37°C. Another possibility is that the surface of the microtubule offers considerable structural flexibility to allow multilevel redundancy to evolve. Given the critical role of the cortical microtubules in generating functional daughter cells (Stokkermans *et al.*, 1996; Shaw *et al.*, 2000; Morrissette and Sibley, 2002b; Morrissette *et al.*, 2004; Fichera *et al.*, 2003; Hu *et al.*, 2006; Hu, 2008), it is reasonable for the parasite to have built-in redundancy to ensure that this key structural framework remains functional in case one mechanism fails. This underlies the need for genome-wide searches for genes that act synergistically, which is now a tractable proposal since clustered regularly interspaced short palindromic repeats (CRISPR)-Cas9–based screens have been established for *T. gondii* (Sebastian Lourido, personal communication).

### Coordination between the assembly of the cortical microtubules and mitotic spindle

During the replication of apicomplexan parasites, the nuclear envelope remains intact. Coordination between the construction of the cortical microtubules in the cytoplasm and the assembly of the mitotic spindle in the nucleus is essential for building a functional daughter.

In this work, we observed that the spindle originates from a spot located at the base of the nucleus, although the later phase of spindle and daughter assembly occurs close to the apical side of the nucleus (Supplemental Video S2). Spindle assembly is contemporaneous with the initiation of the cortical microtubules of the daughters, synchronizing chromosome segregation and daughter formation. It was shown previously that knockdown of SFAs—components of fibers that connect centrioles with the apical end of the

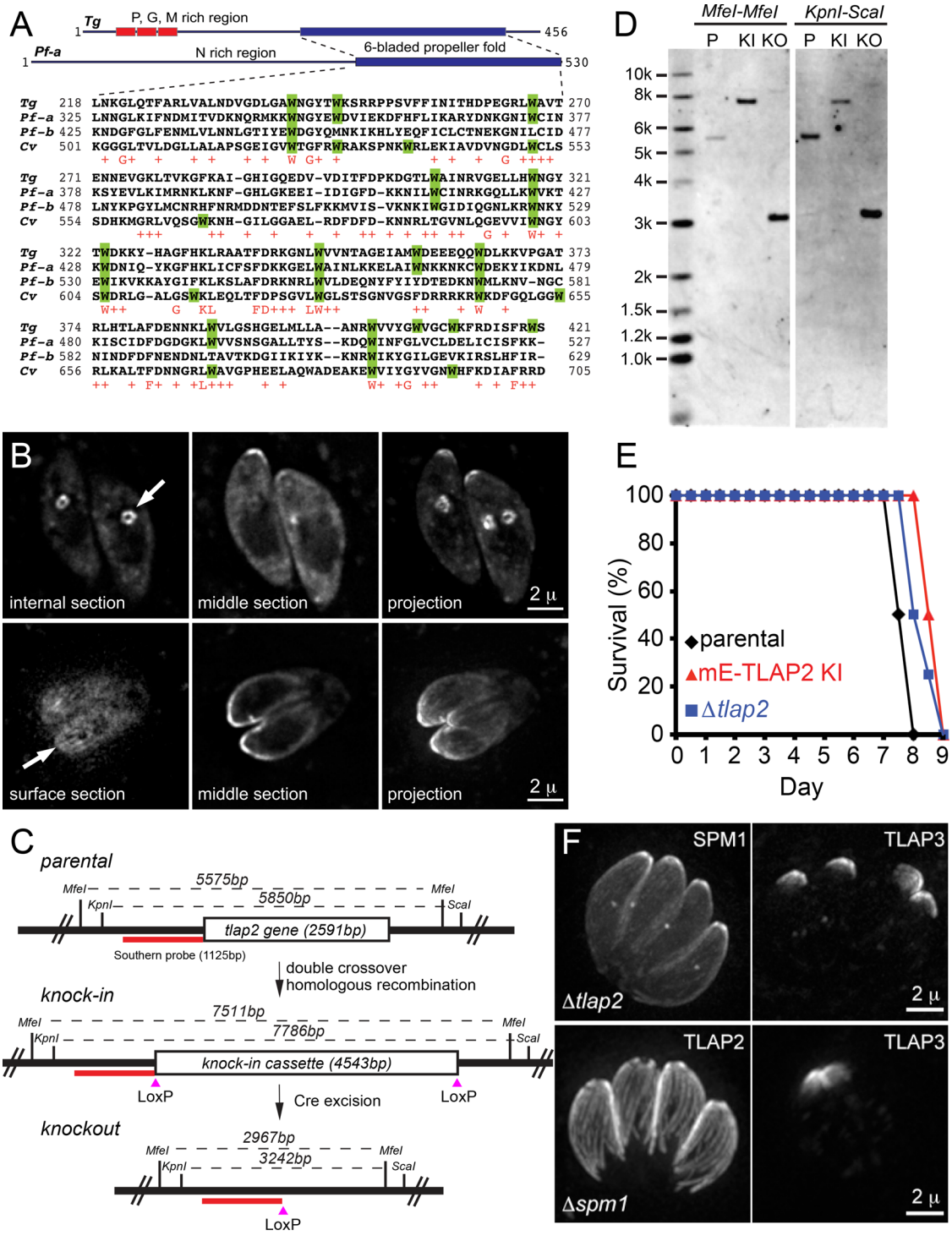
A
Tg
P, G, M rich region
1
456
Pf-a
N rich region
6-bladed propeller fold
1
530
Tg 218 LNKGLQTFARLVALNDVGDLGAWNGYTWKSRRPPSVFFINITHDPEGRLWAVT 270
Pf-a 325 LNNGLKIFNDMITVDKNQRMKKWNGYEWDVIEKDFHFLIKARYDNKGNIWCIN 377
Pf-b 425 KNDGFGLFENMLVLNNLGTIYEWDGYQMNKIKHLYEQFICLCTNEKGNILCID 477
Cv 501 KGGGLTVLDGLLALAPSGEIGVWTGFRWRAKSPNKWRLEKIAVDVNGDLWCLS 553
Tg 271 ENNEVGKLTVKGFKAI-GHIGQEDV-VDITFDPKDGTLWAINRVGELLHWNGY 321
Pf-a 378 KSYEVLKIMRNKLKNF-GHLGKEEI-IDIGFD-KKNILWCINRKGQLLKWVKT 427
Pf-b 478 LNYKPGYLMCNRHFNRMDDNTEFSLFKKMVIS-VKNKIWGIDIQGNLKRWNKY 529
Cv 554 SDHKMGRLVQSGWKNH-GILGGAEL-RDFDFD-KNNRLTGVNLQGEVVIWNGY 603
Tg 322 TWDKKY-HAGFHKLRAATFDRKGNLWVVNTAGEIAMWDEEEQQWDLKKVPGAT 373
Pf-a 428 KWDNIQ-YKGFHKLICFSFDKKGELWAINLKKELAIWNKKNKCWDEKYIKDNL 479
Pf-b 530 EWIKVKKAYGIFKLKSLAFDRKNRLWVLDEQNYFYIYDTEDKNWMLKNV-NGC 581
Cv 604 SWDRLG-ALGSWKLEQLTFDPSGVLWGLSTSGNVGSFDRRRKRWKDFGQLGGW 655
Tg 374 RLHTLAFDENNKLWVLGSHGELMLLA--ANRWVVYGWVGCWKFRDISFRWS 421
Pf-a 480 KISCIDFDGDGKLWVVSNSGALLTYS--KDQWINFGLVCLDELICISFKK- 527
Pf-b 582 NINDFDFNENDNLTAVTKDGIIKIYK--KNRWIKYGILGEVKIRSLHFIR- 629
Cv 656 RLKALTFDNNGRLWAVGPHEELAQWADEAKEWVIYGYVGNWHFKDIAFRRD 705
B
internal section
middle section
projection
2 μ
surface section
middle section
projection
2 μ
C
parental
5575bp
MfeI
KpnI
5850bp
MfeI
ScaI
tlap2 gene (2591bp)
Southern probe (1125bp)
double crossover
homologous recombination
knock-in
7511bp
MfeI
KpnI
7786bp
MfeI
ScaI
knock-in cassette (4543bp)
LoxP
Cre excision
LoxP
knockout
2967bp
MfeI
KpnI
3242bp
MfeI
ScaI
LoxP
D
MfeI-MfeI
KpnI-ScaI
P KI KO P KI KO
10k
8k
6k
5k
4k
3k
2k
1.5k
1.2k
1.0k
E
Survival (%)
100
80
60
40
20
0
parental
mE-TLAP2 KI
Δtlap2
0 1 2 3 4 5 6 7 8 9
Day
F
SPM1
TLAP3
Δtlap2
2 μ
TLAP2
TLAP3
Δspm1
2 μ
G
RHΔhx
Δtlap2
Δtlap2Δspm1
Δtlap2Δspm1Δtlap3

daughter cytoskeleton—inhibits daughter formation but not nuclear division (Francia *et al.*, 2012). It will be interesting to examine how the spindle behaves in SFA-depleted parasites, which may reveal the influence of daughter formation on the dynamics of spindle assembly and growth.

In *ptub-mEmeraldFP-TLAP4* transgenic parasites, the length of TLAP4 labeling of the spindle shortens poleward at late stages of replication, whereas the cortical microtubules continue to elongate. The shortening of TLAP4 decoration on the spindle may coincide with the poleward depolymerization of the spindle. However, it is also possible that dissociation of TLAP4 from the spindle precedes the depolymerization of the spindle microtubules. In either case, this shows that at this stage, polymerization of tubulin on the cortical microtubules is occurring at the same time as depolymerization of microtubules in the spindle. It will be interesting to determine whether and how cell cycle–dependent flux of materials between the cytoplasm and the nucleus—especially the trafficking of tubulins and microtubule-associated proteins—couples the behavior of these two sets of microtubules. The *ptub-mEmeraldFP-TLAP4* transgenic line will be a useful tool for systematically identifying the components of the *T. gondii* spindle, which is critical for elucidating biochemical and biophysical differences between the spindle and cortical microtubules.

In summary, precise spatial and temporal regulation of proteins that associate with microtubules is critical for the biogenesis and function of microtubule-containing apparatuses. The regularity of the *T. gondii* cortical microtubule array and the tractability of its protein coat confer unique advantages for gaining mechanistic insights and developing a more detailed understanding of this process. In addition, simultaneous visualization of mitotic spindle and cortical microtubules in live cells opens the door to understanding how the assembly of cytoskeletal structures in the nucleus and the cytoplasm are coordinated and independently regulated.

## MATERIALS AND METHODS

### *T. gondii* cultures and transfection

The maintenance of *T. gondii* cultures and transfections were carried out as previously described (Liu *et al.*, 2013).

### Mammalian cell cultures and transfection

The maintenance of mammalian cell cultures was carried out as previously described (Liu *et al.*, 2013). The *mCherryFP-Tubulin:eGFP-Histone2B* HeLa cell line was a kind gift from Claire Walczak (Indiana University, Bloomington, IN). For transfection of HFF, HeLa, or Vero cells, JetPEI transfection reagent (101-05; PolyPlus Transfection, Illkirch, France) was used with the conditions recommended by the manufacturer and described in Liu *et al.* (2013).

### Mouse infection experiments

The 4- to 6-wk-old female BALB/c mice were purchased from Harlan Laboratories (Indianapolis, IN) and housed at the Indiana University School of Medicine animal facility in accordance with Institutional Animal Care and Use Committee guidelines for animal care. Intracellular parasites were harvested from an HFF monolayer using syringe passage, filtered, and resuspended in phosphate-buffered saline (PBS). Mice were infected via intraperitoneal injection with 500 tachyzoites in a volume of 100 µl of PBS. A portion of the inoculum was used in a plaque assay and confirmed that equal numbers of parasites were injected into mice. Infected mice were monitored twice daily, and the percentage surviving was recorded.

### Generating the list of TLAP2 homologues and phylogenetic analysis

The C-terminal region of TgTLAP2 (181–456 aa in TGGT1_232130) was used to query the annotated protein databases for apicomplexan parasites and chromerids at EuPathDB.org (Release 25, July 23, 2015) using the BLASTP program and expected (*E*) value 2 as

FIGURE 9: TLAP2 is conserved between *T. gondii, Plasmodium* spp., and *C. velia* and is dispensable for parasite growth. (A) Multiple sequence alignments of the C-terminal domains of TLAP2 homologues from *T. gondii* (TGGT1_232130), *P. falciparum* (-a, PF3D7_1034300 and -b, PF3D7_0517200), and *C. velia* (Cvel_2610). Tryptophan residues are highlighted in green. The consensus of the conserved residues is shown in the bottom row in red. (B) Deconvolved wide-field images of *T. gondii* transiently expressing mEmeraldFP-PfTLAP2-a from a *T. gondii* tubulin promoter. (C) Scheme for generating Δ*tlap2* parasites and Southern blotting strategy. RHΔ*hx* parasites (parental; top) were used to generate *mEmeraldFP-TLAP2* knock-in parasites (knock-in; middle) via double-crossover homologous recombination. The knock-in parasites were then transiently transfected with a plasmid expressing Cre recombinase to excise the genomic fragment between the two LoxP sites. mEmeraldFP(-) parasites were sorted by FACS to facilitate the cloning of Δ*tlap2* parasites (knockout; bottom). The positions of restriction sites and probe (red bar) used in Southern blotting (D) and the corresponding DNA fragment sizes are indicated. (D) Southern blotting analyses of the *tlap2* locus in parental RHΔ*hx* (P), *mEmeraldFP-TLAP2* knock-in (KI), and Δ*tlap2* (KO) parasites generated as described in A. Genomic DNA of the parasites was digested with either *Mfe*I (left) or *Kpn*I-*Sca*I (right). A probe (red bar in C) hybridized to the upstream region of *tlap2* gene was used for the Southern blotting. The predicted *Mfe*I-*Mfe*I fragment size recognized by the probe is 5575 base pairs for RHΔ*hx*, 7511 base pairs for *mEmeraldFP-TLAP2* knock-in, and 2967 base pairs for Δ*tlap2* parasites. The predicted *Kpn*I-*Sca*I fragment size recognized by the probe is 5850 base pairs for RHΔ*hx*, 7786 base pairs for *mEmeraldFP-TLAP2* knock-in, and 3242 base pairs for Δ*tlap2* parasites. (E) Analyses of the virulence of Δ*tlap2* parasites in mice. Each survival curve represents data from a group of four mice infected with an equal number of RHΔ*hx* (parental), *mEmeraldFP-TLAP2* knock-in (mE-TLAP2 KI), or Δ*tlap2* parasites. Mice infected with the parental RHΔ*hx* parasites died between days 7 and 8 postinfection, whereas mice infected with *mEmeraldFP-TLAP2* knock-in or Δ*tlap2* parasites died between days 8 and 9 postinfection. (F) Projections of deconvolved wide-field images showing proper targeting of several coating proteins in Δ*tlap2* and Δ*spm1* parasites. Top, Δ*tlap2* parasites transiently expressing fluorescently tagged SPM1 or TLAP3. Bottom, Δ*spm1* parasites transiently expressing fluorescently tagged TLAP2 or TLAP3. The fluorescently tagged proteins were driven by the 2-kb genomic region immediately upstream of the respective genes in the pTKO2_II vector backbone. Scale bars, 2 µm. (G) Plaque assay of parental RHΔ*hx*, Δ*tlap2*, Δ*tlap2*Δ*spm1*, and Δ*tlap2*Δ*spm1*Δ*tlap3* parasites. HFF cultures were infected with an equal number of each line of parasites, grown for 7 d at 37°C, and then fixed and stained with crystal violet. Host cells remaining attached absorbed the crystal violet staining, whereas regions of host cells lysed by the parasites ("plaques"; arrows) were clear.

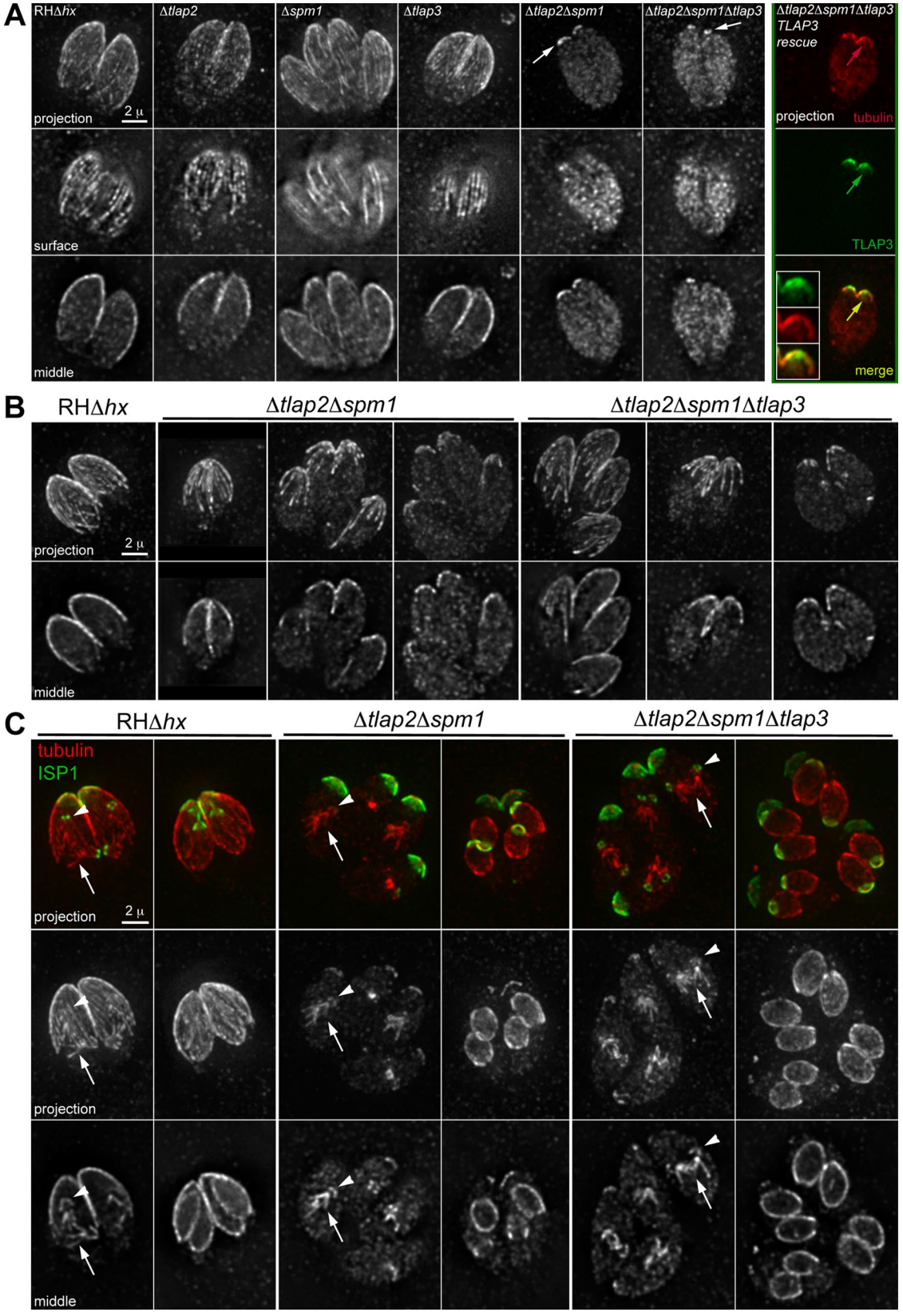


FIGURE 10: The coating proteins protect the stability of cortical microtubules as an ensemble. (A) Deconvolved wide-field images of cold-treated parental RHΔ*hx* parasites and various coating protein–knockout mutants labeled with a rabbit anti–Tgβ-tubulin antibody (Morrissette and Sibley, 2002b). Intracellular parasites were incubated at 8°C for 3.5 h before processing for immunofluorescence. In the Δ*tlap2*Δ*spm1*Δ*tlap3*-TLAP3 rescue parasites, mNeonGreenFP-TLAP3 expression was driven by the 2-kb genomic region immediately upstream of *tlap3* in the plasmid pTKO2_II_ mNeonGreenFP-TLAP3. Insets, 2×. Arrows indicate residual cortical labeling by the anti–Tgβ-tubulin antibody in the

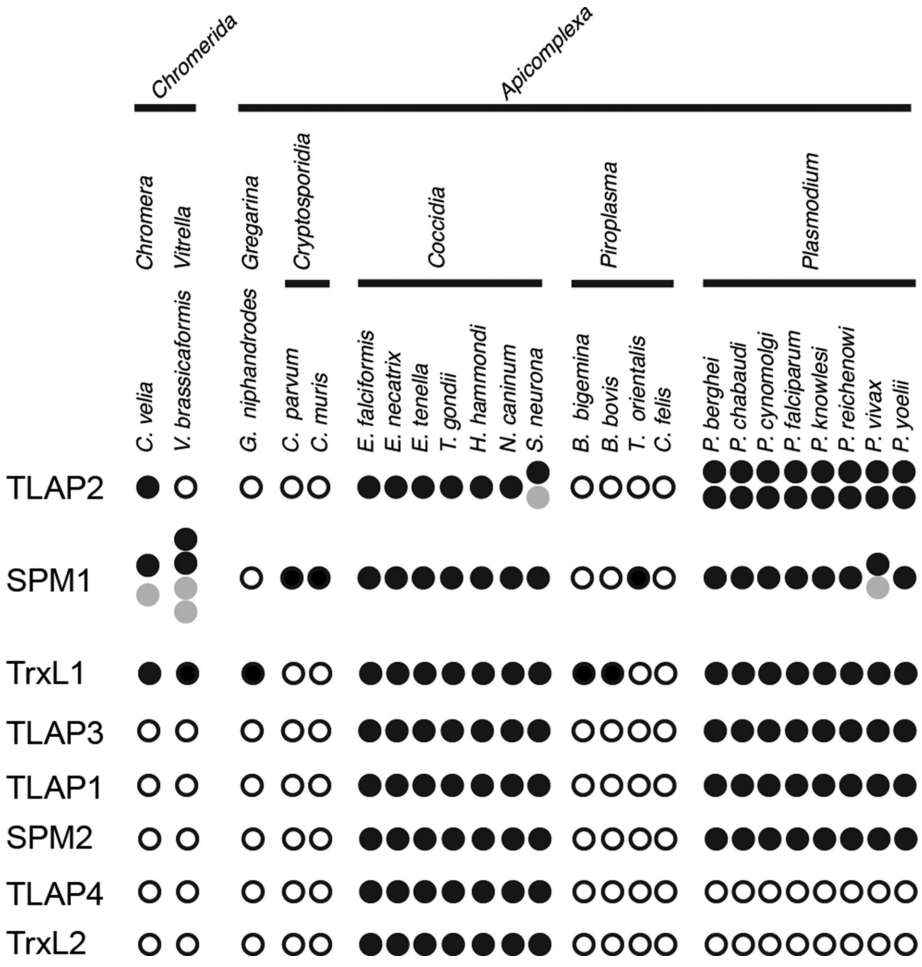


FIGURE 11: Distribution of microtubule-coating proteins in apicomplexan parasites and their photosynthetic relatives. The presence (filled circle) or absence (open circle) of predicted homologues for proteins associated with the cortical microtubules in *T. gondii* in representative members of the phylum Apicomplexa with available genome sequences and its two photosynthetic relatives, *C. velia* and *Vitrella brassicaformis*. Gray circles, predicted proteins whose sequence appears truncated or duplicated due to incomplete assembly. Full-length *T. gondii* homologues were used for the initial BLAST search against the predicted protein databases (eupathdb.org/eupathdb/). *E*-value cut-off, 0.005. For TLAP3 and SPM2, several divergent *Plasmodium* homologues were not captured in the initial BLAST search but were confirmed by using the sequences for more conserved *Plasmodium* homologues as the query. For TrxL1 and TrxL2, due to the conserved nature of the thioredoxin-like fold, only hits with *E*-value <1*e*-18 were considered, and hits with *E*-value between 1*e*-30 and 1*e*-18 were manually curated to classify as TrxL1 or TrxL2 homologues.

the cutoff. Thirty-three TLAP2 homologues were identified. They were aligned using the T-Coffee-WS program accessed through Jalview (version 2.8.1; www.jalview.org) with default parameters to delineate the homologous regions. Multiple alignment of the identified homologous domains was reiterated using T-Coffee WS with default parameters. The phylogenetic tree was then calculated using a neighbor-joining algorithm based on percentage identity by Jalview and displayed using the FigTree program (tree.bio.ed.ac.uk/software/figtree).

### Plasmid construction

All PCR primers, synthesized fragments, and restriction enzymes used for subcloning are listed in Supplemental Table S1, parts 1 and 2. All PCR-generated fragments used for subcloning were verified by sequencing.

### *T. gondii* expression plasmids

ptub-mEmeraldFP-TLAP2, ptub-mEmeraldFP-TLAP3, and ptub-mEmeraldFP-TLAP4: The coding sequences (CDSs) of TLAP2, TLAP3, or TLAP4 without the start codon were individually amplified from a cDNA library isolated from RH parasites by PCR to generate products with appropriate restriction sites at each end. Amplified TLAP2 CDS was digested with *Bgl*II-*Afl*II, and TLAP3 and TLAP4 CDSs were digested with *Bgl*II-*Rsr*II and subcloned into the corresponding sites on the ptub-mEmeraldFP-TgTrxL1_50_178aa backbone (Liu *et al.*, 2013).

ptub-mEmeraldFP-PfTLAP2-a: The CDS of PfTLAP2-a gene, which has no introns, was amplified from 3D7A *P. falciparum* genomic DNA (MRA-151G; MR4, Manassas, VA) by PCR to generate a product without the start codon and with *Bgl*II and *Afl*II sites at the 5′ and 3′ ends, respectively. The amplified CDS was digested with *Bgl*II-*Afl*II and subcloned into the same sites on the ptub-mEmeraldFP-TgTrxL1_50_178aa backbone (Liu *et al.*, 2013).

ptub-mAppleFP-TLAP2: mAppleFP CDS was amplified using the mAppleFP-C1 plasmid (Kremers *et al.*, 2009) as the template by PCR to generate a product with mAppleFP CDS followed by the coding sequence for a GHGTGSTGSTSSRS linker and *Nhe*I and *Bgl*II sites at the 5′ and 3′ ends, respectively. The PCR product was digested with *Nhe*I-*Bgl*II and subcloned in the same sites on ptub-mEmeraldFP-TLAP2 to replace the coding sequence for mEmeraldFP.

ptub-mAppleFP-TLAP4: A DNA fragment encoding mAppleFP and a GHGTGSTGSTSSRS linker was released from plasmid ptub-mAppleFP-TLAP2 using *Nhe*I-*Bgl*II digestion and subcloned into the *Nhe*I-*Bgl*II sites on ptub-mEmeraldFP-TLAP4 to replace the coding sequence for mEmeraldFP.

pTKO2-II-mEmeraldFP-TLAP2: The ~2-kb fragments immediately upstream or downstream of the *tlap2* locus were amplified by PCR using genomic DNA isolated from RH parasites as the template, and the mEmeraldFP-TLAP2 fusion gene was amplified by PCR using ptub-mEmeraldFP-TLAP2 as the template while adding

Δ*tlap2*Δ*spm1*, Δ*tlap2*Δ*spm1*Δ*tlap3*, or Δ*tlap2*Δ*spm1*Δ*tlap3*- TLAP3 rescue parasites. (B, C) Deconvolved wide-field images of intracellular parental RHΔ*hx*, Δ*tlap2*Δ*spm1*, and Δ*tlap2*Δ*spm1*Δ*tlap3* parasites labeled with a rabbit anti–Tgβ-tubulin antibody. The parasites were cultured under standard culture conditions (i.e., with no cold treatment) before processing for immunofluorescence. (B) Interphase parasites. (C) Parasites with forming daughters (arrows, mitotic spindle; green, anti-ISP1; red, anti–Tgβ-tubulin).

the *tlap2* Kozak sequence at the 5′ end. The upstream and downstream genomic sequences and Kozak-mEmeraldFP-TLAP2 fusion gene were successively subcloned into the *Not*I-*Xho*I, *Hin*dIII-*Nhe*I, and *Asi*SI-*Rsr*II sites on pTKO2-II-mCherryFP (Liu *et al.*, 2013) plasmid backbone, respectively.

pTKO2-II-mEmeraldFP-TLAP3: The ~2-kb fragments immediately upstream or downstream of the *tlap3* locus were amplified by PCR using genomic DNA isolated from RH parasites as the template, and the mEmeraldFP-TLAP3 fusion gene was amplified by PCR using ptub-mEmeraldFP-TLAP3 as the template to generate a product with the Kozak sequence of *tlap3* at the 5′ end. The fragments for the upstream and downstream genomic sequences, and Kozak-mEmeraldFP-TLAP3 fusion gene were successively subcloned into the *Not*I-XhoI, *Hpa*I-*Psp*OMI, and *Pme*I-*Rsr*II sites on the pTKO2-II-mCherryFP plasmid backbone, respectively.

pTKO2-II-mNeonGreenFP-TLAP3: A DNA fragment coding for mNeonGreenFP, SGLRS linker, and the N-terminal part of TLAP3 up to a *Sgr*DI site was synthesized (GenScript, Piscataway, NJ; Supplemental Table S1), digested with *Pme*I and *Sgr*DI, and subcloned into the *Pme*I-*Sgr*DI sites on pTKO2-II-mEmeraldFP-TLAP3 to replace the coding sequence for mEmeraldFP with that for mNeonGreenFP.

pTKO2-II-mEmeraldFP-SPM1: The ~2-kb fragments immediately upstream or downstream of the *spm1* locus were amplified by PCR using genomic DNA isolated from RH parasites as the template, and SPM1 CDS was amplified by PCR using a RH parasite cDNA library to generate a product with the Kozak sequence of *spm1* at the 5′ end. The downstream and upstream genomic sequences and Kozak-SPM1 fragments were successively subcloned into the *Apa*I-*Nhe*I, *Not*I-*Eco*RV, and *Bgl*II-*Rsr*II sites on the pTKO2-II-mCherryFP plasmid backbone, respectively. This produced an intermediate plasmid pTKO2-II-SPM1. Subsequently a DNA fragment containing the coding sequences for mEmeraldFP, SGLGS linker, and the N-terminus region of SPM1 was synthesized (GenScript; Supplemental Table S1), digested with *Bgl*II and *Xma*I, and subcloned into the *Bgl*II-*Xma*I sites on pTKO2-II-SPM1 to produce pTKO2-II-mEmeraldFP-SPM1 in which the coding sequence for mEmeraldFP was placed N-terminal to the SPM1 CDS.

pmin-Cre-eGFP_Gra-mCherry: A Cre-eGFP expression cassette including a *dhfr* promoter and the *dhfr* 3′ untranslated region was released from the plasmid pmin-Cre-eGFP (Heaslip *et al.*, 2010) by *Apa*I-*Not*I digestion and subcloned into the *Apa*I-*Not*I site on pTKO2-II-mCherryFP to replace the DHFR expression cassette.

pmin-mEmeraldFP-TgCentrin1: The CDS of TgCentrin1 (TGGT1_247230; EuPathDB.org) was amplified by PCR using a cDNA library isolated from RH parasites as the template. The product was digested with *Bgl*II-*Afl*II and subcloned into the *Bgl*II-*Afl*II sites on a pmin-mEmeraldFP plasmid backbone, which was first produced by using the coding sequence for mEmeraldFP to replace that for mCherryFP in pmin-mCherryFP-TgMORN1 (Hu, 2008).

### Bacterial expression plasmids

pET22b(+)-FLAG-TLAP2 and pET22b(+)-FLAG-TLAP2_181-456aa: DNA fragments encoding full-length TLAP2 minus the start codon or TLAP2_181-456aa were amplified by PCR using ptub-mEmeraldFP-TLAP2 as the template, digested with *Nhe*I and *Not*I, and subcloned into the *Nhe*I-*Not*I sites on a pET22b(+)-FLAG plasmid backbone as described previously (Liu *et al.*, 2013).

### Mammalian cell expression plasmids

pC22-mEmeraldFP-TLAP2: A DNA fragment encoding mEmeraldFP-TLAP2 was released from ptub-mEmeraldFP-TLAP2 by *Nhe*I-*Afl*II digestion and subcloned into the *Nhe*I-*Afl*II sites on pC22-EGFP-TrxL1 (Liu *et al.*, 2013) to replace eGFP-TrxL1.

pC22-mEmeraldFP-TLAP3: A DNA fragment encoding mEmeraldFP-TLAP3 was released from ptub-mEmeraldFP-TLAP3 by *Nhe*I-*Afl*II digestion and subcloned into the *Nhe*I-*Afl*II sites on pC22-eGFP-TrxL1 (Liu *et al.*, 2013) to replace eGFP-TrxL1.

pC22-mEmeraldFP-TLAP4: The TLAP4 CDS without the start codon was amplified by PCR using ptub-mEmeraldFP-TLAP4 as the template to generate a product with *Bgl*II and *Apa*I sites at the 5′ and 3′ ends, respectively. The PCR product was digested with *Bgl*II and *Apa*I and subcloned in the *Bgl*II-*Apa*I sites flanking the TLAP2 CDS fragment on pC22-mEmeraldFP-TLAP2 to replace the TLAP2 CDS fragment.

### Generation of transgenic, knock-in, and knockout parasites

*mEmeraldFP-TLAP2* knock-in parasite: RHΔ*hx* parasites, ~$1 \times 10^7$, were electroporated with 30 μg of pTKO2-II-mEmeraldFP-TLAP2 plasmid linearized with *Not*I, selected with 25 μg/ml mycophenolic acid and 50 μg/ml xanthine for two passages, and cloned by FACS for mEmeraldFP(+)/mCherryFP(-) parasites. All clones were confirmed with diagnostic genomic PCRs as previously described (Liu *et al.*, 2013), and three of them were further verified by Southern blotting. One of the verified clones was used in imaging and the subsequent generation of Δ*tlap2* parasites.

*mNeonGreenFP-TLAP3* knock-in parasite: RHΔ*ku80*Δ*hx* parasites, ~$1 \times 10^7$ (Fox *et al.*, 2009; Huynh and Carruthers, 2009; a kind gift from Vern Carruthers, University of Michigan, Ann Arbor, MI), were electroporated with 40 μg of pTKO2-II-mNeonGreenFP-TLAP3 plasmid linearized with *Sap*I, selected with 25 μg/ml mycophenolic acid and 50 μg/ml xanthine, and cloned by FACS for mNeonGreenFP(+)/mCherryFP(-) parasites. Three clones were confirmed with diagnostic genomic PCRs as previously described (Liu *et al.*, 2013), and one of them was further verified by Southern blotting. The verified clone was used in imaging and the subsequent generation of Δ*tlap3* parasites.

*ptub-mEmeraldFP-TLAP4* transgenic parasite: RHΔ*hx* parasites, ~$1 \times 10^7$, were electroporated with 30 μg of ptub-mEmeraldFP-TLAP4 plasmid, selected with 20 μM chloramphenicol, and cloned by FACS. One clone was used exclusively in this study.

*ptub-mEmeraldFP-TLAP4:pmin-mTagRFP-TgMORN1* transgenic parasite: *ptub-mEmeraldFP-TLAP4* parasites, ~$1 \times 10^7$, were electroporated with a mixture of 20 μg of pmin-mTagRFP-TgMORN1 and 20 μg of pC3 (for expressing a pyrimethamine-resistant DHFR allele; Donald and Roos, 1993) plasmids together and selected with 1 μM pyrimethamine.

Δ*tlap2* parasite: *mEmeraldFP-TLAP2* knock-in parasites, ~$1 \times 10^7$, were electroporated with 20 μg of pmin-Cre-eGFP_Gra-mCherry, selected with 80 μg/ml 6-thioxanthine for two passages, and cloned by FACS for mEmeraldFP(-)/mCherryFP(+) parasites in which the mEmeraldFP-TLAP2 coding region and the HXGPRT cassette were excised. The transient mCherryFP expression from pmin-Cre-eGFP_Gra-mCherry was used to distinguish live parasites from cell debris. All clones were confirmed with diagnostic genomic PCRs as previously described (Liu *et al.*, 2013), and two of them were further verified by Southern blotting. One of the verified clones was used in analysis and the subsequent generation of Δ*tlap2*Δ*spm1* parasites.

Δ*tlap3* parasite: *mNeonGreenFP-TLAP3* knock-in parasites, ~$1 \times 10^7$, were electroporated with 20 μg of pmin-Cre-eGFP_Gra-mCherry, selected with 80 μg/ml 6-thioxanthine, and cloned by FACS as described. One clone was confirmed with diagnostic genomic PCRs as previously described (Liu *et al.*, 2013) and further verified by Southern blotting.

Δ*tlap2:mEmeraldFP-SPM1* knock-in parasite: Δ*tlap2* parasites, ~$1 \times 10^7$, were electroporated with 30 µg of pTKO2-II-mEmeraldFP-SPM1 plasmid linearized with *Not*I, selected with 25 µg/ml mycophenolic acid and 50 µg/ml xanthine until parasites were resistant to the drug, and cloned by FACS for mEmeraldFP(+)/mCherryFP(-) parasites. Two clones were confirmed with diagnostic genomic PCRs as previously described (Liu *et al.*, 2013). One of them was further verified by Southern blotting and used in analysis and the subsequent generation of Δ*tlap2*Δ*spm1* parasites.

Δ*tlap2*Δ*spm1* parasite: Δ*tlap2:mEmeraldFP-SPM1* knock-in parasites, ~$1 \times 10^7$, were electroporated with 20 µg of pmin-Cre-eGFP_Gra-mCherry, selected with 80 µg/ml 6-thioxanthine for two passages until parasites were resistant to the drug, and cloned by limited dilution in 96-well plates. Four clones were confirmed with diagnostic genomic PCRs as previously described (Liu *et al.*, 2013). One of them was further verified by Southern blotting and used in subsequent analysis and the generation of Δ*tlap2*Δ*spm1:mNeonGreenFP-TLAP3* knock-in parasites.

Δ*tlap2*Δ*spm1:mNeonGreenFP-TLAP3* knock-in parasite: Δ*tlap2*Δ*spm1* parasites, ~$1 \times 10^7$, were electroporated with 20 µg of pTKO2-II-mNeonGreen-TLAP3 plasmid, selected with 25 µg/ml mycophenolic acid and 50 µg/ml xanthine for three passages, and cloned by FACS for mNeonGreenFP(+)/mCherryFP(-) parasites. Two clones were confirmed with diagnostic genomic PCRs as previously described (Liu *et al.*, 2013). One of them was further verified by Southern blotting and used in analysis and the subsequent generation of Δ*tlap2*Δ*spm1*Δ*tlap3* parasites.

Δ*tlap2*Δ*spm1*Δ*tlap3* parasite: Δ*tlap2*Δ*spm1:mNeonGreenFP-TLAP3* knock-in parasites, ~$1 \times 10^7$, were electroporated with 20 µg of pmin-Cre-eGFP_Gra-mCherry, selected with 80 µg/ml 6-thioxanthine for two passages, and cloned by limited dilution in 96-well plates. Three clones were confirmed with diagnostic genomic PCRs as previously described (Liu *et al.*, 2013). One of them was further verified by Southern blotting and used in subsequent analysis.

### FACS and parasite cloning

FACS was carried out using an AriaII flow cytometer (BD Biosciences, San Jose, CA) at the flow cytometry core facility at Indiana University (Bloomington, IN). For cloning, three parasites with desired fluorescence profile were sorted per well of a 96-well plate containing a monolayer of HFF host cells. Wells containing single plaques were screened 7 d after sorting.

### Southern blotting

Southern blotting was conducted as previously described (Liu *et al.*, 2013) and detected using the Phototope-Star detection kit (N7020; New England BioLabs). All probes were synthesized using the NEBlot Phototope kit (N7550; New England BioLabs, Ipswich, MA). PCR primers and templates, and restriction fragments used for generating probes for Southern blotting analyses are listed in Supplemental Table S1, parts 3 and 4.

To determine the change in the *tlap2* locus in *mEmeraldFP-TLAP2* knock-in and Δ*tlap2* parasites, genomic DNA was digested with *Mfe*I alone or *Kpn*I-*Sca*I. An 1125–base pair fragment immediately upstream of *tlap2* was released from plasmid pTKO2-II-mEmeraldFP-TLAP2 by *Sac*I-*Bgl*II digestion and used as the template in probe synthesis.

To determine the change in the *tlap3* locus in *mNeonGreenFP-TLAP3* knock-in and Δ*tlap3* parasites, genomic DNA was digested with *Bam*HI(HF)-*Ase*I or *Bam*HI(HF)-*Nco*I. For the *Bam*HI(HF)-*Ase*I digestion, a 1075–base pair fragment upstream of *tlap3* was amplified by PCR from plasmid pTKO2-II-mEmeraldFP-TLAP3 and used as the template in probe synthesis. For the *Bam*HI(HF)-*Nco*I digestion, a 535–base pair fragment upstream of *tlap3* was released from pTKO2-II-mEmeraldFP-TLAP3 by *Bgl*II-*Nco*I digestion and used as the template in probe synthesis.

To determine the change in the *spm1* locus in Δ*tlap2:mEmeraldFP-SPM1* knock-in and Δ*tlap2*Δ*spm1* parasites, genomic DNA was digested with *Sac*I(HF). A 563–base pair CDS fragment and a 697–base pair downstream fragment of *spm1* were amplified by PCR from pTKO2-II-mEmeraldFP-SPM1 and used as the template in probe synthesis for the CDS and downstream probes, respectively.

To determine the change in the *tlap3* locus in Δ*tlap2*Δ*spm1:mNeonGreenFP-TLAP3* knock-in and Δ*tlap2*Δ*spm1*Δ*tlap3* parasites, genomic DNA was digested with *Ase*I-*Xba*I. A 202–base pair CDS fragment and a 1075–base pair upstream fragment of *tlap3* were amplified by PCR from plasmid pTKO2-II-mEmeraldFP-TLAP3 and used as the template in probe synthesis for the CDS and upstream probes, respectively.

### Cold treatment of *T. gondii* for testing microtubule stability

Cultures of intracellular parasites growing in HFF cells in 3.5-cm glass-bottom dishes (P35G-1.5-20-C; MatTek, Ashland, MA) were incubated at 8°C for 3.5 h in $CO_2$-independent medium (Hu *et al.*, 2006; RR060058; Life Technologies, Carlsbad, CA) supplemented with 1% (vol/vol) heat-inactivated cosmic calf serum (CCS; SH30087.3; Hyclone, Logan, UT), GlutaMAX (35050-061; Life Technologies), sodium pyruvate (11360; Life Technologies), and antibiotic/antimycotic (30-004-CI; Corning, Oneonta, NY). The samples were then processed for immunofluorescence as described next.

### Immunofluorescence

All immunofluorescence labeling steps were performed at room temperature unless otherwise indicated.

For intracellular parasites, *T. gondii*–infected HFF monolayers growing in a 3.5-cm glass-bottom dish were fixed in 3.7% (vol/vol) formaldehyde in PBS for 15 min, permeabilized in 0.5% (vol/vol) Triton X-100 (TX-100) in PBS for 15 min, and blocked in 1% (wt/vol) bovine serum albumin (BSA) in PBS for ~30 min, followed by antibody labeling (see later description). Dishes were incubated in primary antibodies for ~0.5–1 h and then in secondary antibodies for ~0.5–1 h unless otherwise noted. Primary antibodies and dilutions used were as follows: rabbit anti-IMC1, 1:1000 (a kind gift from Con Beckers, University of North Carolina, Chapel Hill, NC; Mann and Beckers, 2001); mouse anti-ISP1 1:1000 (a kind gift from Peter Bradley, University of California, Los Angeles, CA; Beck *et al.*, 2010); rat anti-TLAP2 1:10 (purified using anti-serum produced by Cocalico Biologicals [Reamstown, PA]); and rabbit anti–Tgβ1-tubulin (Morrissette and Sibley, 2002b), 1:1000 (incubation for 2 h at room temperature or overnight at 8°C). Secondary antibodies and dilutions used were goat anti-rabbit immunoglobulin G (IgG) Cy5, 1:1000 (111-175-144; Jackson ImmunoResearch, West Grove, PA); goat anti-rabbit IgG Cy3, 1:1000 (111-165-144; Jackson ImmunoResearch); goat anti-mouse IgG Cy3 1:1000 (115-165-166; Jackson ImmunoResearch); and goat anti-rat IgG Alexa 568, 1:1000 (A11077, Life Technologies-Molecular Probes, Eugene, OR). The nucleic acid counterstain Hoechst 33342 (H-1399; Life Technologies-Molecular Probes) was used at 4 µg/ml.

For labeling of microtubules in extracellular parasites, ~$1 \times 10^7$ parasites were concentrated to ~10 µl, spotted onto clean Parafilm, and overlaid with a poly-L-lysine (P8920; Sigma-Aldrich, St. Louis, MO)–coated coverslip for 30 min. The parasites were then extracted with 1% (wt/vol) sodium deoxycholate for 20 min or 0.5% (vol/vol) TX-100 for 40 min and fixed in 3.7% (vol/vol) formaldehyde in PBS

for 15 min or methanol for 5 min. Coverslips were blocked with 1% (wt/vol) BSA in PBS for 30 min. The samples were then incubated for 60 min first in a mouse anti–α-tubulin (T6074; Sigma-Aldrich) and anti–β-tubulin (T5293; Sigma-Aldrich) mixture at 1:1000 each and subsequently in goat anti-mouse IgG Cy3 (A11031; Molecular Probes) at 1:1000.

Immunofluorescence labeling of the microtubule cytoskeleton in mammalian cells was performed as described previously (Liu *et al.*, 2013). A mixture of mouse anti–α-tubulin (T6074; Sigma-Aldrich) and anti–β-tubulin (T5293; Sigma-Aldrich) diluted at 1:1000 each was used as the primary antibody, and goat anti-mouse IgG Cy3 (A11031; Molecular Probes) at 1:1000 was used as the secondary antibody.

### Recombinant FLAG-TLAP2 and FLAG-TLAP2_181-456aa expression and purification

Production of recombinant FLAG-TLAP2 and FLAG-TLAP2_181-456aa was performed using a procedure reported previously (Liu *et al.*, 2013). Briefly, pET22b(+)-FLAG-TLAP2 or pET22b(+)-FLAG-TLAP2_181-456aa was transformed into BL21-CodonPlus(DE3)RP strain *E. coli* (230255; Stratagene, Santa Clara, CA). Protein expression was induced with 1 mM isopropyl-β-D-thiogalactoside for 16 h at 20°C. The induced *E. coli* culture was pelleted and lysed in lysis buffer (25 mg/ml CelLytic express [C1990; Sigma-Aldrich], 150 mM NaCl, 0.5 mM EDTA, 2.5 mM dithiothreitol [DTT], 0.5% [vol/vol] TX-100, 1% [vol/vol] glycerol, and protease inhibitors in 20 mM Tris-HCl, pH 8). The recombinant protein was affinity purified from the lysate with M2-FLAG agarose resin (A2220; Sigma-Aldrich), eluted with 100 μg/ml FLAG peptide (F3290; Sigma-Aldrich), and concentrated with an Amicon 10k MWCO centrifugal filter (501096; Millipore, Billerica, MA). The purified protein was used fresh or stored in 40% glycerol with elution buffer at –80 or –20°C.

### Antibody production and affinity purification

Polyclonal rat anti-TLAP2 serum was produced by Cocalico Biologicals. A mixture of purified FLAG-TLAP2_181-456aa recombinant protein in solution (see earlier description) and in SDS–PAGE gel slices was used as antigen.

### In vitro microtubule-binding assay

Microtubules were polymerized from 16 μM tubulin (MT240; Cytoskeleton, Denver, CO) in 1× KAcE buffer (10 mM Tris($CH_3COO$), 50 mM K($CH_3COO$), 4 mM $MgSO_4$, 1 mM ethylene glycol tetraacetic acid, pH 7.5) supplemented with 20 μM paclitaxel in dimethyl sulfoxide, 0.5 mM GTP, and 2 mM DTT at 37°C for 30 min. Microtubules at an equivalent concentration of 0.5 μM tubulin dimer were mixed with a buffer control or 0.25 μM FLAG-TLAP2_2-456aa recombinant protein at room temperature. The reaction was injected immediately into a micro slide chamber, which was assembled by gluing a #1 coverslip (18 × 18 mm; Matsunami, Tokyo, Japan) to a precleaned microscope slide using strips of Scotch double-sided tape (core series 2-4600; 3M, St. Paul, MN) and imaged using dark-field microscopy (see later description).

### Live-cell imaging

Unless otherwise noted, for live-cell imaging, the parasites were kept in $CO_2$-independent medium (Hu *et al.*, 2006) supplemented with 1% (vol/vol) heat-inactivated CCS and GlutaMAX, sodium pyruvate, and antibiotic/antimycotic.

### Three-dimensional structured-illumination microscopy

Three-dimensional structured-illumination microscopy (3D-SIM) image stacks were collected at *z*-increments of 0.125 μm using an OMX imaging station (GE Healthcare-Applied Precision, Seattle, WA). A 100× oil immersion lens (numerical aperture [NA] 1.40) and immersion oil at refractive index 1.516 or 1.518 were used. Deconvolved images were computed using the point-spread functions and software supplied by the manufacturer.

### Dark-field microscopy

Dark-field illumination was arranged using the output from a 100-W Hg arc lamp filtered to remove ultraviolet and infrared wavelengths and installed on the transmitted light mount of an inverted microscope (IMT2; Olympus, Shinjuku, Japan), with a Zeiss oil immersion NA 1.2/1.4 cardioid condenser and imaging through an objective lens with NA < 1.2 (typically, a 20×/NA 0.8 Olympus DPlanApo UV). Microtubules in aqueous buffer were adsorbed to the surface of a slide coupled to the condenser with immersion oil, thus taking advantage of the evanescent field generated at the glass/water interface by the high-angle illumination, NA > 1.33, as well as the far-field illumination provided by light at lower angles (1.2 < NA < 1.33). Images were captured using a Qimaging Retiga EX camera.

### Wide-field deconvolution microscopy

The 3D image stacks were collected at 35–37°C using a DeltaVision imaging station (GE Healthcare-Applied Precision) constructed on an Olympus IX-70 inverted microscope base. A 100 or 60× oil immersion lens and immersion oil at refractive index 1.518–1.524 or a 60× silicone oil immersion lens (Olympus 60× UApoN NA 1.3) was used for the imaging.

### Fluorescence recovery after photobleaching

FRAP experiments were performed on a DeltaVision RT imaging system equipped with an environmental chamber held at 37°C and a 488-nm laser connected to the microscope via a 1-mm-diameter fiber optic. The collimated laser beam was introduced into the back aperture of the imaging lens (Olympus 60× UApoN NA 1.3 silicone immersion), yielding a diffraction-limited spot at the sample of 0.08–0.3 mW. A single 35-ms pulse was used for photobleaching, which was sufficient to reduce the fluorescence by 60–80%. Prebleaching and postbleaching images were collected using the photokinetics module integrated in the Applied Precision Softworx software. Images were collected with a pixel spacing of 0.11 μm. Three images were collected immediately before the bleach pulse and 3–10 at 0.5- to 15-s intervals after the pulse. To monitor longer-term recovery, movement of the parasites made it necessary to collect 3D stacks to ensure an in-focus view. Stacks of six images with a *z*-spacing of 0.5 μm were collected at 5- to 15-min intervals for 1–8 h after the pulse, depending on the recovery rate. After collection of the images needed to measure fluorescence recovery, the targeted parasites were imaged at infrequent intervals for 6–8 h to ensure that they were capable of proceeding normally through the next round of daughter formation and cell division.

The photobleaching rate of mNeonGreenFP-TLAP3 due entirely to the imaging illumination, without a laser pulse, was measured in independent experiments on our microscope system and found to be accurately modeled by a single-exponential decay process. Under the conditions used here, 101 s of imaging illumination was needed to reduce fluorescence of mNeonGreen-TLAP3 to one-half of its initial value. In the time-lapse experiments, the highest total cumulative imaging exposure was <90 s, and the average cumulative total was ~40 s. Fluorescence decay due to the imaging illumination was corrected in the analyses as described next.

For quantitative analysis of FRAP experiments, regions of interest (ROIs) were manually drawn around each target region (with a small

extra margin to allow for blurring due to small amounts of defocus), several nontarget control regions, and a nearby extracellular background region, using the image analysis program FIJI (Schindelin *et al.*, 2012; fiji.sc/Fiji). The patches of TLAP3 analyzed by FRAP in these experiments are small enough (<1 µm thick) to be quantitatively represented by measurements on a single plane, provided that the plane is within ~1 µm of optimal focus. Every ROI was manually reassigned, in the plane of optimal focus, at every time point to compensate for cell movement during the experiment.

The gray levels of all pixels within each ROI were summed to give the raw measurements. Corrections were applied to the raw measurements to compensate for variations in lamp output, using the output from the photosensor on the DeltaVision system that monitors and integrates actual illumination intensity during the nominally constant exposure times. The similarly compensated background fluorescence was then subtracted from each ROI. The ROIs were all near the center of the field of view, and variation in illumination intensity across the field of view was small enough that attempted compensation for the spatial variation ("flat-fielding") actually caused a decrease in signal-to-noise ratio rather than an improvement (i.e., introduced more variance due to noise amplification than was removed by compensating for the small amount of spatial variation). The cumulative exposure time was tracked throughout each experiment, allowing quantitative correction for losses in fluorescence due merely to the imaging illumination, specifically for each optical section in each 3D stack at each time point. Finally, division of the corrected sum of gray levels within each ROI by the actual exposure time for the corresponding image (as monitored by the photosensor) converted these sums into true intensities (i.e., gray levels/s) so that measurements from different experiments using different nominal exposure times can be directly compared. For reference, an increment of 1 in gray level corresponds to approximately six photons captured by the camera on our system.

### Image processing

The brightness and contrast of images used in the final figures were optimized for color printing. The gamma value for the lookup table was adjusted for images in Figures 4, 5, and 8 and Supplemental Video S2 because they contain features with a wide range of intensities. Adjustments were made such that weak signals can be displayed without saturating the strong signals. These adjustments did not eliminate any signals captured in the original image.

### Plaque assays

Plaque assays were performed as previously described (Heaslip *et al.*, 2010). A total of 50, 75, 100, 150, or 200 parasites was added to each well of 12-well plates with confluent HFF monolayers and grown undisturbed for 7 d, then fixed with cold methanol for 15 min and stained with 1% (wt/vol) crystal violet in 25% (vol/vol) methanol.

## ACKNOWLEDGMENTS

We thank Peter Bradley (University of California, Los Angeles) for the mouse anti-ISP1 antibody, Con Beckers (University of North Carolina, Chapel Hill) for the rabbit anti-IMC1 antibody, Claire Walczak (Indiana University) for the mCherryFP-tubulin:eGFP-Histone2B HeLa cell line, Vern Carruthers (University of Michigan) for the RHΔ*ku80*Δ*hx* parasites, Jacqueline Leung (Indiana University) for critical readings of the manuscript and insightful discussions, and Amanda Rollins for technical support. This study was supported by funding from the March of Dimes (6-FY15-198), the National Institutes of Health/National Institute of Allergy and Infectious Diseases (R01-AI098686) awarded to K.H., and facility and fellowship funding from the Indiana Clinical and Translational Sciences Institute to K.H. and J.L., funded in part by Grants UL1 TR001108 and TL1TR001107 from a National Institutes of Health, National Center for Advancing Translational Sciences, Clinical and Translational Sciences Award. I.B. was supported by National Institutes of Health Grant T32 AI060519. This research was supported in part by the National Science Foundation under Grant No. NSF PHY11-25915 to the Kavli Institute of Theoretical Physics (KITP) at the University of California, Santa Barbara, and by the Gordon and Betty Moore Foundation under Award No. 2919 to the KITP.

## REFERENCES

Abdrakhamanova A, Wang QY, Khokhlova L, Nick P (2003). Is microtubule disassembly a trigger for cold acclimation? Plant Cell Physiol 44, 676–686.

Aikawa M, Carter R, Ito Y, Nijhout MM (1984). New observations on gametogenesis, fertilization, and zygote transformation in *Plasmodium gallinaceum*. J Protozool 31, 403–413.

Arnette C, Efimova N, Zhu X, Clark GJ, Kaverina I (2014). Microtubule segment stabilization by RASSF1A is required for proper microtubule dynamics and Golgi integrity. Mol Biol Cell 25, 800–810.

Bannister LH, Mitchell GH (1995). The role of the cytoskeleton in *Plasmodium falciparum* merozoite biology: an electron-microscopic view. Ann Trop Med Parasitol 89, 105–111.

Barisic M, Silva e Sousa R, Tripathy SK, Magiera MM, Zaytsev AV, Pereira AL, Janke C, Grishchuk EL, Maiato H (2015). Mitosis. Microtubule detyrosination guides chromosomes during mitosis. Science 348, 799–803.

Beazley DM, Egerman RS (1998). Toxoplasmosis. Semin Perinatol 22, 332–338.

Beck JR, Rodriguez-Fernandez IA, de Leon JC, Huynh M-H, Carruthers VB, Morrissette NS, Bradley PJ (2010). A novel family of *Toxoplasma* IMC proteins displays a hierarchical organization and functions in coordinating parasite division. PLoS Pathog 6, e1001094.

Bernhard W, De Harven E (1956). Electron microscopic study of the ultrastructure of centrioles in vertebra [in French]. Z Zellforsch Mikrosk Anat 45, 378–398.

Binder LI, Frankfurter A, Rebhun LI (1985). The distribution of tau in the mammalian central nervous system. J Cell Biol 101, 1371–1378.

Bulinski JC, Richards JE, Piperno G (1988). Posttranslational modifications of alpha tubulin: detyrosination and acetylation differentiate populations of interphase microtubules in cultured cells. J Cell Biol 106, 1213.

Caceres A, Binder LI, Payne MR, Bender P, Rebhun L, Steward O (1984). Differential subcellular localization of tubulin and the microtubule-associated protein MAP2 in brain tissue as revealed by immunocytochemistry with monoclonal hybridoma antibodies. J Neurosci 4, 394–410.

Carvalho-Santos Z, Azimzadeh J, Pereira-Leal JB, Bettencourt-Dias M (2011). Evolution: tracing the origins of centrioles, cilia, and flagella. J Cell Biol 194, 165–175.

Chen AL, Kim EW, Toh JY, Vashisht AA, Rashoff AQ, Van C, Huang AS, Moon AS, Bell HN, Bentolila LA, *et al.* (2015). Novel components of the *Toxoplasma* inner membrane complex revealed by BioID. MBio 6, e02357.

Chobotar W, Scholtyseck E (1982). Ultrastructure. In: The Biology of the Coccidia, ed. PL Long, Baltimore, MD: University Park Press, 101–165.

De Storme N, Copenhaver GP, Geelen D (2012). Production of diploid male gametes in *Arabidopsis* by cold-induced destabilization of postmeiotic radial microtubule arrays. Plant Physiol 160, 1808–1826.

Detrich HW, Parker SK, Williams RC, Nogales E, Downing KH (2000). Cold adaptation of microtubule assembly and dynamics. Structural interpretation of primary sequence changes present in the alpha- and beta-tubulins of Antarctic fishes. J Biol Chem 275, 37038–37047.

D'Haese J, Mehlhorn H, Peters W (1977). Comparative electron microscope study of pellicular structures in coccidia (*Sarcocystis*, *Besnoitia* and *Eimeria*). Int J Parasitol 7, 505–518.

Dobrowolski JM, Carruthers VB, Sibley LD (1997). Participation of myosin in gliding motility and host cell invasion by *Toxoplasma gondii*. Mol Microbiol 26, 163–173.

Dobrowolski JM, Sibley LD (1996). *Toxoplasma* invasion of mammalian cells is powered by the actin cytoskeleton of the parasite. Cell 84, 933–939.

Donald RG, Roos DS (1993). Stable molecular transformation of *Toxoplasma gondii*: a selectable dihydrofolate reductase-thymidylate synthase

marker based on drug-resistance mutations in malaria. Proc Natl Acad Sci USA 90, 11703–11707.
Douzery EJP, Snell EA, Bapteste E, Delsuc F, Philippe H (2004). The timing of eukaryotic evolution: does a relaxed molecular clock reconcile proteins and fossils? Proc Nat Acad Sci USA 101, 15386–15391.
Dubey JP (1998). Advances in the life cycle of *Toxoplasma gondii*. Int J Parasitol 28, 1019–1024.
Dubey JP (2008). The history of *Toxoplasma gondii*—the first 100 years. J Eukaryot Microbiol 55, 467–475.
Dubey JP, Miller NL, Frenkel JK (1970). The *Toxoplasma gondii* oocyst from cat feces. J Exp Med 132, 636–662.
Dubremetz JF (1973). Etude ultrastructurale des mitoses et de l'organitogenese au cours de la schizogonie chez la coccidie *Eimeria necatrix*, sporozoaire parasite du poulet domestique. These de troisieme cycle. Lille, France: Universite des Sciences et Techniques de Lille I Laboratoire de Biologie Animale.
Dubremetz JF, Torpier G (1978). Freeze fracture study of the pellicle of an Eimerian sporozoite (Protozoa, Coccidia). J Ultrastruct Res 62, 94–109.
Dunn D, Wallon M, Peyron F, Petersen E, Peckham C, Gilbert R (1999). Mother-to-child transmission of toxoplasmosis: risk estimates for clinical counselling. Lancet 353, 1829–1833.
Dutcher SK (2003). Elucidation of basal body and centriole functions in *Chlamydomonas reinhardtii*. Traffic 4, 443–451.
Egarter S, Andenmatten N, Jackson AJ, Whitelaw JA, Pall G, Black JA, Ferguson DJP, Tardieux I, Mogilner A, Meissner M (2014). The *Toxoplasma* Acto-MyoA motor complex is important but not essential for gliding motility and host cell invasion. PLoS One 9, e91819.
Escalante AA, Ayala FJ (1995). Evolutionary origin of *Plasmodium* and other Apicomplexa based on rRNA genes. Proc Nat Acad Sci USA 92, 5793–5797.
Fichera ME, Oh J, Lilley P, Brown E, Roos DS (2003). Dinitroaniline herbicide resistance in *Toxoplasma gondii*. Presented at 7th International Congress on Toxoplasmosis, Tarrytown, NY.
Fowler RE, Fookes RE, Lavin F, Bannister LH, Mitchell GH (1998). Microtubules in *Plasmodium falciparum* merozoites and their importance for invasion of erythrocytes. Parasitology 117, 425–433.
Fox BA, Ristuccia JG, Gigley JP, Bzik DJ (2009). Efficient gene replacements in *Toxoplasma gondii* strains deficient for nonhomologous end joining. Eukaryot Cell 8, 520–529.
Francia ME, Jordan CN, Patel JD, Sheiner L, Demerly JL, Fellows JD, de Leon JC, Morrissette NS, Dubremetz J-F, Striepen B (2012). Cell division in Apicomplexan parasites is organized by a homolog of the striated rootlet fiber of algal flagella. PLoS Biol 10, e1001444.
Frenkel JK (1973). Toxoplasmosis: Parasite Life Cycle, Pathology, and Immunology, Baltimore, MD: University Park Press.
Fung C, Beck JR, Robertson SD, Gubbels M-J, Bradley PJ (2012). *Toxoplasma* ISP4 is a central IMC sub-compartment protein whose localization depends on palmitoylation but not myristoylation. Mol Biochem Parasitol 184, 99–108.
Gaskins E, Gilk S, DeVore N, Mann T, Ward G, Beckers C (2004). Identification of the membrane receptor of a class XIV myosin in *Toxoplasma gondii*. J Cell Biol 165, 383–393.
Gibbons IR (1981). Cilia and flagella of eukaryotes. J Cell Biol 91, 107s–124s.
Gilbert SP, Allen RD, Sloboda RD (1985). Translocation of vesicles from squid axoplasm on flagellar microtubules. Nature 315, 245–248.
Heaslip AT, Dzierszinski F, Stein B, Hu K (2010). TgMORN1 is a key organizer for the basal complex of *Toxoplasma gondii*. PLoS Pathog 6, e1000754.
Heaslip AT, Nishi M, Stein B, Hu K (2011). The motility of a human parasite, *Toxoplasma gondii*, is regulated by a novel lysine methyltransferase. PLoS Pathog 7, e1002201.
Hoff EF, Carruthers VB (2002). Is *Toxoplasma* egress the first step in invasion? Trends Parasitol 18, 251–255.
Hu K (2008). Organizational changes of the daughter basal complex during the parasite replication of *Toxoplasma gondii*. PLoS Pathog 4, 108–121.
Hu K, Johnson J, Florens L, Fraunholz M, Suravajjala S, DiLullo C, Yates J, Roos DS, Murray JM (2006). Cytoskeletal components of an invasion machine—the apical complex of *Toxoplasma gondii*. PLoS Pathog 2, 0121–0139.
Hu K, Mann T, Striepen B, Beckers CJ, Roos DS, Murray JM (2002a). Daughter cell assembly in the protozoan parasite *Toxoplasma gondii*. Mol Biol Cell 13, 593–606.
Hu K, Roos DS, Murray JM (2002b). A novel polymer of tubulin forms the conoid of *Toxoplasma gondii*. J Cell Biol 156, 1039–1050.
Huitorel P (1988). From cilia and flagella to intracellular motility and back again: a review of a few aspects of microtubule-based motility. Biol Cell 63, 249–258.
Huynh MH, Carruthers VB (2009). Tagging of endogenous genes in a *Toxoplasma gondii* strain lacking Ku80. Eukaryotic Cell 8, 530–539.
Inoué S, Fuseler J, Salmon ED, Ellis GW (1975). Functional organization of mitotic microtubules. Physical chemistry of the in vivo equilibrium system. Biophys J 15, 725–744.
Inoué S, Sato H (1967). Cell motility by labile association of molecules: the nature of mitotic spindle fibers and their role in chromosome movement. J Gen Physiol 50, 259–292.
Janke C, Kneussel M (2010). Tubulin post-translational modifications: encoding functions on the neuronal microtubule cytoskeleton. Trends Neurosci 33, 362–372.
Jasmin BJ, Changeux JP, Cartaud J (1990). Compartmentalization of cold-stable and acetylated microtubules in the subsynaptic domain of chick skeletal muscle fibre. Nature 344, 673–675.
Johnson KA, Rosenbaum JL (1992). Replication of basal bodies and centrioles. Curr Opin Cell Biol 4, 80–85.
Kan A, Tan Y-H, Angrisano F, Hanssen E, Rogers KL, Whitehead L, Mollard VP, Cozijnsen A, Delves MJ, Crawford S, *et al*. (2014). Quantitative analysis of *Plasmodium* ookinete motion in three dimensions suggests a critical role for cell shape in the biomechanics of malaria parasite gliding motility. Cell Microbiol 16, 734–750.
Konishi Y, Setou M (2009). Tubulin tyrosination navigates the kinesin-1 motor domain to axons. Nat Neurosci 12, 559–567.
Kreitzer G, Liao G, Gundersen GG (1999). Detyrosination of tubulin regulates the interaction of intermediate filaments with microtubules in vivo via a kinesin-dependent mechanism. Mol Biol Cell 10, 1105–1118.
Kremers GJ, Hazelwood KL, Murphy CS, Davidson MW, Piston DW (2009). Photoconversion in orange and red fluorescent proteins. Nat Methods 6, 355–358.
Kumar N, Aikawa M, Grotendorst C (1985). *Plasmodium gallinaceum*: critical role for microtubules in the transformation of zygotes into Ookinetes. Exp Parasitol 59, 239–247.
Kuo C-H, Wares JP, Kissinger JC (2008). The Apicomplexan whole-genome phylogeny: an analysis of incongruence among gene trees. Mol Biol Evol 25, 2689–2698.
Leung JM, Rould MA, Konradt C, Hunter CA, Ward GE (2014). Disruption of TgPHIL1 alters specific parameters of *Toxoplasma gondii* motility measured in a quantitative, three-dimensional live motility assay. PLoS One 9, e85763.
Levine ND (1988). Progress in taxonomy of the Apicomplexan protozoa. J Protozool 35, 518–520.
Liu J, Wetzel L, Zhang Y, Nagayasu E, Ems-McClung S, Florens L, Hu K (2013). Novel thioredoxin-like proteins are components of a protein complex coating the cortical microtubules of *Toxoplasma gondii*. Eukaryot Cell 12, 1588–1599.
Luder CG, Bohne W, Soldati D (2001). Toxoplasmosis: a persisting challenge. Trends Parasitol 17, 460–463.
Luduena RF (1998). Multiple forms of tubulin: different gene products and covalent modifications. Int Rev Cytol 178, 207–275.
Luft BJ, Hafner R, Korzun AH, Leport C, Antoniskis D, Bosler EM, Bourland DDd, Uttamchandani R, Fuhrer J, Jacobson J (1993). Toxoplasmic encephalitis in patients with the acquired immunodeficiency syndrome. Members of the ACTG 077p/ANRS 009 Study Team. N Engl J Med 329, 995–1000.
Luft BJ, Remington JS (1992). Toxoplasmic encephalitis in AIDS. Clin Infect Dis 15, 211–222.
Mann T, Beckers C (2001). Characterization of the subpellicular network, a filamentous membrane skeletal component in the parasite *Toxoplasma gondii*. Mol Biochem Parasitol 115, 257–268.
Mann T, Gaskins E, Beckers C (2002). Proteolytic processing of TgIMC1 during maturation of the membrane skeleton of *Toxoplasma gondii*. J Biol Chem 277, 41240–41246.
Meissner M, Schluter D, Soldati D (2002). Role of *Toxoplasma gondii* myosin A in powering parasite gliding and host cell invasion. Science 298, 837–840.
Montoya JG, Liesenfeld O (2004). Toxoplasmosis. Lancet 363, 1965–1976.
Morejohn LC, Bureau TE, Mole-Bajer J, Bajer AS, Fosket DE (1987). Oryzalin, a dinitroaniline herbicide, binds to plant tubulin and inhibits microtubule polymerization *in vitro*. Planta 172, 252–264.
Morrissette NS (1995). The Apical Cytoskeleton of *Toxoplasma gondii:* Structural and Biochemical Characterization of Elements Associated with the Conoid and Subpellicular Microtubules. PhD Dissertation. Philadelphia: University of Pennsylvania.

Morrissette NS, Mitra A, Sept D, Sibley LD (2004). Dinitroanilines bind alpha-tubulin to disrupt microtubules. Mol Biol Cell 15, 1960–1968.
Morrissette NS, Murray JM, Roos DS (1997). Subpellicular microtubules associate with an intramembranous particle lattice in the protozoan parasite *Toxoplasma gondii*. J Cell Sci 110, 35–42.
Morrissette NS, Sibley LD (2002a). Cytoskeleton of apicomplexan parasites. Microbiol Mol Biol Rev 66, 21–38.
Morrissette NS, Sibley LD (2002b). Disruption of microtubules uncouples budding and nuclear division in *Toxoplasma gondii*. J Cell Sci 115, 1017–1025.
Nichols BA, Chiappino ML (1987). Cytoskeleton of *Toxoplasma gondii*. J Protozool 34, 217–226.
Nishi M, Hu K, Murray JM, Roos DS (2008). Organellar dynamics during the cell cycle of *Toxoplasma gondii*. J Cell Sci 121, 1559–1568.
Opitz C, Soldati D (2002). "The glideosome": a dynamic complex powering gliding motion and host cell invasion by *Toxoplasma gondii*. Mol Microbiol 45, 597–604.
Oropesa-Avila M, Fernandez-Vega A, de la Mata M, Garrido-Maraver J, Cotan D, Paz MV, Pavon AD, Cordero MD, Alcocer-Gomez E, de Lavera I, *et al.* (2014). Apoptotic cells subjected to cold/warming exposure disorganize apoptotic microtubule network and undergo secondary necrosis. Apoptosis 19, 1364–1377.
Papasozomenos SC, Binder LI, Bender PK, Payne MR (1985). Microtubule-associated protein 2 within axons of spinal motor neurons: associations with microtubules and neurofilaments in normal and beta,beta'-iminodipropionitrile-treated axons. J Cell Biol 100, 74–85.
Pinder J, Fowler R, Bannister L, Dluzewski A, Mitchell GH (2000). Motile systems in malaria merozoites: how is the red blood cell invaded? Parasitol Today 16, 240–245.
Pollister AW (1939). Centrioles and chromosomes in the atypical spermatogenesis of *Vivipara*. Proc Natl Acad Sci USA 25, 189–195.
Porchet E, Torpier G (1977). Etude du germe infectieux de *Sarcocystis tenella* et *Toxoplasma gondii* par la technique du cryodecapage. Z Parasitenkd 54, 101–124.
Preble AM, Giddings TM Jr, Dutcher SK (2000). Basal bodies and centrioles: their function and structure. Curr Top Dev Biol 49, 207–233.
Rosenbaum J (2000). Cytoskeleton: functions for tubulin modifications at last. Curr Biol 10, R801–R803.
Salisbury JL (1995). Centrin, centrosomes, and mitotic spindle poles. Curr Opin Cell Biol 7, 39–45.
Salmon ED (1975). Spindle microtubules: thermodynamics of in vivo assembly and role in chromosome movement. Ann NY Acad Sci 253, 383–406.
Salmon ED, Begg DA (1980). Functional implications of cold-stable microtubules in kinetochore fibers of insect spermatocytes during anaphase. J Cell Biol 85, 853–865.
Sawin KE, Mitchison TJ (1991). Poleward microtubule flux mitotic spindles assembled in vitro. J Cell Biol 112, 941–954.
Schindelin J, Arganda-Carreras I, Frise E, Kaynig V, Longair M, Pietzsch T, Preibisch S, Rueden C, Saalfeld S, Schmid B, *et al.* (2012). Fiji: an open-source platform for biological-image analysis. Nat Methods 9, 676–682.
Senaud J (1967). Contribution a l'etude des *Sarcosporidies* et des *Toxoplasmes* (*Toxoplasmea*). Protistologica 3, 167–232.
Shaw MK, Compton HL, Roos DS, Tilney LG (2000). Microtubules, but not actin filaments, drive daughter cell budding and cell division in *Toxoplasma gondii*. J Cell Sci 113, 1241–1254.
Sheetz MP, Vale R, Schnapp B, Schroer T, Reese TS (1986). Vesicle movements and microtubule-based motors. J Cell Sci Suppl 5, 181–188.
Sheffield HG, Melton ML (1968). The fine structure and reproduction of *Toxoplasma gondii*. J Parasitol 54, 209–226.
Sibley L, Dobrowski J, Morisaki J, Heuser J (1994). Invasion and intracellular survival by *Toxoplasma gondii*. In: Bailliere's Clinical Infectious Diseases, Vol. 1, ed. D Russell, London: Bailliere Tindall, 245–264.
Sibley LD (2004). Intracellular parasite invasion strategies. Science 304, 248–253.
Sibley LD, Hakansson S, Carruthers VB (1998). Gliding motility: an efficient mechanism for cell penetration. Curr Biol 8, R12–R14.
Sinden RE (1985). A cell biologist's view of host cell recognition and invasion by malarial parasites. Trans R Soc Trop Med Hyg 79, 598–605.
Stebbings H, Hunt C (1987). The translocation of mitochondria along insect ovarian microtubules from isolated nutritive tubes: a simple reactivated model. J Cell Sci 88, 641–648.
Stephens RE (1992). Tubulin in sea urchin embryonic cilia: post-translational modifications during regeneration. J Cell Sci 101, 837–845.
Stokkermans TJ, Schwartzman JD, Keenan K, Morrissette NS, Tilney LG, Roos DS (1996). Inhibition of *Toxoplasma gondii* replication by dinitroaniline herbicides. Exp Parasitol 84, 355–370.
Sullivan WJ Jr, Jeffers V (2012). Mechanisms of *Toxoplasma gondii* persistence and latency. FEMS Microbiol Rev 36, 717–733.
Swedlow JR, Hu K, Andrews PD, Roos DS, Murray JM (2002). Measuring tubulin content in *Toxoplasma gondii*: a comparison of laser-scanning confocal and wide-field fluorescence microscopy. Proc Natl Acad Sci USA 99, 2014–2019.
Szollosi D (1964). The structure and function of centrioles and their satellites in the jellyfish *Phialidium gregarium*. J Cell Biol 21, 465–479.
Torgerson PR, Mastroiacovo P (2013). The global burden of congenital toxoplasmosis: a systematic review. Bull World Health Org 91, 501–508.
Tran JQ, Li C, Chyan A, Chung L, Morrissette NS (2012). SPM1 stabilizes subpellicular microtubules in *Toxoplasma gondii*. Eukaryot Cell 11, 206–216.
Vanderberg J, Rdodin J, Yoeli M (1967). Electron microscopic and histochemical studies of sporozoite formation in *Plasmodium berghei*. J Protozool 14, 82–103.
Walczak CE, Heald R (2008). Mechanisms of mitotic spindle assembly and function. Int Rev Cytol 265, 111–158.
Westermann S, Weber K (2003). Post-translational modifications regulate microtubule function. Nat Rev Mol Cell Biol 4, 938–948.
World Health Organization (2014). World Malaria Report 2014, Geneva.
Zhu X-P, You F, Zhang P-J, Xu Y-L, Xu J-H (2006). Effects of cold shock on microtubule organization and cell cycle in gynogenetically activated eggs of olive flounder (*Paralichthys olivaceus*). Mar Biotechnol (NY) 8, 312–318.